MOUNTAIN-PLAINS CONSORTIUM

MPC 24-536 | S. Ni, A. Sorensen, I. Unobe and A. Pokhrel

IMPACT OF VEHICLE FIRES ON POLYMER CONCRETE BRIDGE DECK OVERLAYS

MOUNTAIN-PLAINS CONSORTIUM REGION 8

A University Transportation Center sponsored by the U.S. Department of Transportation serving the Mountain-Plains Region. Consortium members:

Colorado State University
North Dakota State University
South Dakota State University
University of Colorado Denver
University of Denver
University of Utah
Utah State University
University of Wyoming

Technical Report Documentation Page

1. Report No.	2. Government Accession No.	3. Recipient's Catalog No.
MPC-663		

4. Title and Subtitle	5. Report Date
Impact of Vehicle Fires on Polymer Concrete Bridge Deck Overlays	July 2024
	6. Performing Organization Code

7. Author(s)	8. Performing Organization Report No.
Shuna Ni Andrew D. Sorensen Ikwulono David Unobe Ashesh Pokhrel	MPC 24-536

9. Performing Organization Name and Address	10. Work Unit No. (TRAIS)
Utah State University Department of Civil & Environmental Engineering 4110 Old Main Hill Logan, UT 84322-4110	11. Contract or Grant No.

12. Sponsoring Agency Name and Address	13. Type of Report and Period Covered
Mountain-Plains Consortium North Dakota State University PO Box 6050, Fargo, ND 58108	Final Report
	14. Sponsoring Agency Code

15. Supplementary Notes

Supported by a grant from the US DOT, University Transportation Centers Program

16. Abstract

Polymer concrete (PC) has found increasing use in construction over the last few decades. One common use of this material is as an overlay material on bridges and highways. This use can be attributed to some advantages of this material such as its high bond strength with substrate concrete, short curing times, good resistance to water and chlorine penetration, and excellent skid and abrasion resistance. However, PC is susceptible to degradation upon exposure to elevated temperatures. Thus, it has become necessary to accurately characterize its behavior under such conditions and propose remedies to limit the deterioration. This study set out to do this, by carrying out a vehicle fire test on a slab with PC overlaid on it. Performance properties, including skid resistance, surface hardness, resistance to water and chloride penetration, abrasion resistance, bond strength and resistance to delamination, were utilized to characterize the behavior of this material before and after exposure to the vehicle fire. The results showed a significant decrease in performance across all parameters after exposure to the elevated temperatures. As a remedy, this study suggested the application of an intumescent coating, which uses a blend of fire-retardant materials (including expandable graphite, aluminum trihydrate and calcium carbonate) mixed into polyester binder resin, to cover the surface of the PC. Preliminary tests indicate that this method holds promise for mitigating the rapid deterioration of PC when exposed to elevated temperatures.

17. Key Word	18. Distribution Statement
Bridge decks, concrete bridges, polymer concrete, vehicle fire, fire resistance	Public distribution

19. Security Classif. (of this report)	20. Security Classif. (of this page)	21. No. of Pages	22. Price
Unclassified	Unclassified	82	n/a

Form DOT F 1700.7 (8-72) Reproduction of completed page authorized

Impact of Vehicle Fires on Polymer Concrete Bridge Deck Overlays

Shuna Ni

Andrew D. Sorensen

Ikwulono David Unobe

Ashesh Pokhrel

Utah State University

Logan, Utah

July 2024

Ackowledgements

The authors acknowledge the US Department of Transportation through the Mountain-Plains Consortium (MPC) for funding this research. The authors also acknowledge the Cache Valley Fire Department for providing space and logistics for the vehicle fire test, as well as Granite construction for constructing the overlay. In addition, the authors would also like to acknowledge a good number of colleagues and peers who provided valuable assistance and advice during this project.

Disclaimer

The contents of this report reflect the views of the authors, who are responsible for the facts and the accuracy of the information presented. This document is disseminated under the sponsorship of the Department of Transportation, University Transportation Centers Program, in the interest of information exchange. The U.S. Government assumes no liability for the contents or use thereof.

North Dakota State University does not discriminate in its programs and activities on the basis of age, color, gender expression/identity, genetic information, marital status, national origin, participation in lawful off-campus activity, physical or mental disability, pregnancy, public assistance status, race, religion, sex, sexual orientation, spousal relationship to current employee, or veteran status, as applicable. Direct inquiries to Vice Provost, Title IX/ADA Coordinator, Old Main 100, (701) 231-7708, ndsu.eoaa@ndsu.edu.

ABSTRACT

Polymer concrete (PC) has found increasing use in construction over the last few decades. One common use of this material is as an overlay material on bridges and highways. This use can be attributed to some advantages of this material such as its high bond strength with substrate concrete, short curing times, good resistance to water and chlorine penetration, and excellent skid and abrasion resistance. However, PC is susceptible to degradation upon exposure to elevated temperatures. Thus, it has become necessary to accurately characterize its behavior under such conditions and propose remedies to limit the deterioration. This study attempted to achieve this by carrying out a vehicle fire test on a slab with PC overlaid on it. Performance properties, including skid resistance, surface hardness, resistance to water and chloride penetration, abrasion resistance, bond strength and resistance to delamination, were utilized to characterize the behavior of this material before and after exposure to the vehicle fire. The results showed a significant decrease in performance across all parameters after exposure to the elevated temperatures. As a remedy, this study suggested the application of an intumescent coating, which uses a blend of fire-retardant materials (including expandable graphite, aluminum trihydrate and calcium carbonate) mixed into polyester binder resin, to cover the surface of the PC. Preliminary tests indicate that this method holds promise for mitigating the rapid deterioration of PC when exposed to elevated temperatures.

TABLE OF CONTENTS

LIST OF TABLES

LIST OF FIGURES

EXECUTIVE SUMMARY

Polymer concrete (PC), commonly used in highway infrastructure for its numerous advantages, faces significant risks under high temperatures such as those produced by vehicle fires. This vulnerability can lead to the degradation or destruction of PC overlays on bridge decks. The problem is exacerbated by differences in thermal expansion between PC overly and substrate concrete, potentially causing delamination and further damage during uneven heat exposure typical of vehicle fires. The overall objective of this project is to enhance the vehicle fire resistance of PC bridge deck overlays. The specific research objectives are: 1) to identify the impact of vehicle fires on the performance of PC overlay; and 2) to develop effective methods to improve the fire resistance of PC overlays or to protect PC overlays from exposure to vehicle fires.

The research was meticulously planned and executed using a large composite slab, which consists of a conventional cement concrete substrate with polyester polymer concrete overlaid on it, designed according to the UDOT Structures Design & Detailing Manual to emulate a section of a bridge deck. Comprehensive pre-fire testing was carried out on this slab, employing both nondestructive and destructive methods to measure baseline properties of the PC overlay, including skid resistance, surface hardness, abrasion resistance, resistance to water and chloride penetration, bond strength and presence of delamination. A simulated vehicle fire was then conducted on the large slab, replicating an accidental fire outbreak on a bridge deck with a PC overlay. This experiment was designed to mimic real-life conditions as closely as possible, including non-uniform heating and rapid cooling phases, which are typical in actual fire scenarios due to firefighting efforts. Temperatures recorded during the experiment reached up to 1,200°C within the vehicle and 745°C on the surface of the slab, providing a depiction of the severe thermal challenges PC overlays might face during a vehicle fire. A peak heat flux up to 47.5 kW/m^2, measured by a heat flux sensor 12 feet from the center of the vehicle, suggested potential risks of a vehicle fire not only to the immediate pavement but also to adjacent infrastructure, such as suspension bridge cables, and could even trigger wildfires if near flammable areas. Following the fire test, both the pre-established nondestructive and destructive assessments were repeated to evaluate the extent of fire-related damages to the PC overlay's properties. The findings indicated significant degradation in critical PC properties, including skid resistance, surface hardness, abrasion resistance, and resistance to water and chloride penetration. Notably, delamination of the overlay from the underlying concrete was observed, along with pronounced bond failures, particularly in areas that experienced the highest temperatures.

PC overlay degradation under extreme temperatures highlights the need for better fire resistance methods. Traditional approaches typically involve adding fire-resistant materials into the PC mix before casting. However, these methods cannot be utilized in already installed PC overlays, and modifying PC's intrinsic properties could make it less appealing for certain uses. To tackle this, this project developed an intumescent coating that can be applied directly to existing PC overlays. The coating is a blend of fire-retardant materials mixed into polyester binder resin. The coating acts as a protective barrier, insulating the PC from intense heat during vehicle fires and reducing degradation risk. To test this coating's effectiveness, extensive evaluations were conducted on both treated and untreated PC slab samples, simulating the thermal exposure of a typical vehicle fire. These tests assessed critical performance aspects, including skid resistance, surface hardness, resistance to water penetration, abrasion resistance, and resistance to chloride penetration. Results showed that treated PC overlays maintained better performance under heat up to 500°C, exhibiting less degradation compared with untreated overlays. This underscores the coating's potential to significantly enhance the durability of existing PC overlays exposed to high temperatures.

1. INTRODUCTION

1.1 Problem Statement

There were 223,000 vehicle fires in the United States in 2019, with 189,500 occurring on highways [1]. Such fires can result in temperatures exceeding 1,000°F [2], which can cause various levels of damage to highway infrastructure, resulting in interruptions to the transportation network. An example is the oil tanker fire which occurred under an overpass on the I-95 in Philadelphia on June 11, 2023, leading to the collapse of a section of the overpass.

Unconventional materials that incorporate polymers, e.g., polymer concrete (PC) and polymer-modified concrete (PMC), are increasingly used in highway infrastructure projects. PC has characteristics that make it an attractive choice for overlays on existing or new bridges. These include high resistance to chloride and water penetration, excellent freeze-thaw resistance, high chemical stability under corrosive environment, high compressive strength, low shrinkage, and an ability to achieve its maximum strength in a short time [3]. Due to these attractive qualities, the use of PC as overlays on bridges has continued to rapidly increase. By 2016, more than 50 bridges had been protected by PC overlays in Utah [4].

Although PC has attractive properties, the polymer resins used are sensitive to high temperatures, with relatively low glass transition temperatures (Tg) and heat distortion temperatures (HDT). The sensitivity of these materials to elevated temperatures has led to the concern that a vehicle fire could degrade or even completely destroy a PC overlay on a bridge deck. Some further concerns also attend the temperature sensitivity of PC when used as overlays on bridge decks. Among those concerns is the deformation incompatibility between a PC overlay and a concrete substrate at high temperatures. The thickness of a PC overlay is relatively small, usually applied at a total thickness of under one inch [5]. Under a vehicle fire, the PC overlay will be exposed to elevated temperatures while the temperature of the concrete substrate beneath it could remain relatively low, as shown in Figure 1. Such a thermal gradient along the bridge deck may lead to the delamination of the overlay from the concrete substrate. This could be further aggravated by the significant difference in the thermal expansion coefficient of PC and that of conventional cement concrete, which could lead to differences in thermal expansion even under similar temperature exposure [6,7].

While some prior research has focused on the potential negative impacts of the significant difference between the thermal expansion coefficient of PC and that of conventional concrete [6,7], such studies primarily focused on ambient temperature ranges and the exposure of PC to relatively uniform temperature increases or decreases. However, the heat exposure of a PC overlay from a vehicle fire does not fit into such scenarios as the temperatures will be much higher than ambient temperatures. Also, the temperature changes will not be uniform either across the surface or over the duration of exposure. In addition, the composite panel experiences thermal gradients not only along its thickness (as illustrated by the vertical red arrow in Figure 1.1), but also along its surface (the horizontal red arrow) due to the low thermal conductivity of materials and the non-uniform heat exposure of a surface under a vehicle fire. Such gradients along a panel surface may result in overlays directly exposed to a vehicle fire expanding against the cooler surrounding areas and thus damaging them.

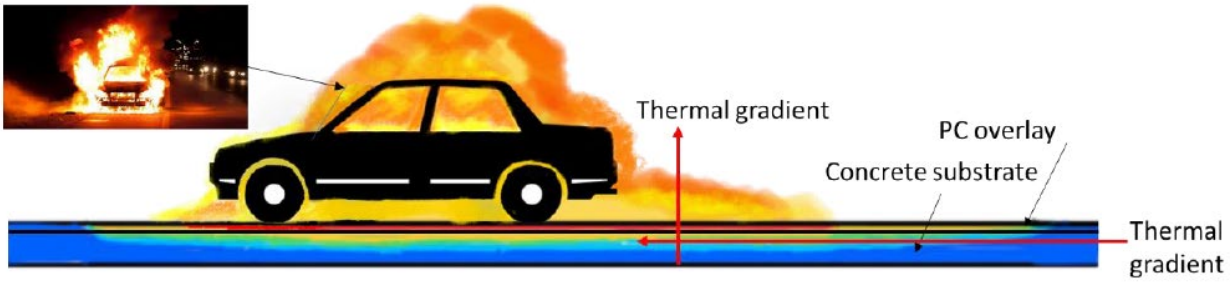

Figure 1.1 Thermal gradient of a bridge deck under a vehicle fire

1.2 Objectives

Limited information exists on how a composite panel, which consists of a conventional cement concrete substrate with PC overlays (hereafter referred to as a "composite slab"), reacts when directly exposed to a vehicle fire. The overall objective of this project is to enhance the vehicle fire resistance of PC bridge deck overlays. The specific research objectives are:

Objective 1: To identify the impact of vehicle fires on PC bridge deck overlays.

Objective 2: To develop effective methods to improve the fire resistance of PC overlays or to protect PC overlays from exposure to vehicle fires.

1.3 Scope

To achieve the laid-out objectives of the project, a number of tasks were planned for execution. Most of the planned work involved experimental tests. These experimental tests included a vehicle fire test on a constructed composite slab with performance tests on the slab before and after the vehicle fire tests. Also planned were controlled tests on smaller composite slabs to test possible solutions for mitigating the degradation of the PC overlay when exposed to extreme temperatures.

The first step toward meeting the stated objectives was to design and construct a reinforced concrete slab and smaller slabs, all overlaid with PC. The larger composite slab, designed to replicate a section of a bridge deck, was designed according to the *UDOT Structures Design & Detailing Manual* [8]. The smaller slabs were designed primarily to test possible solutions for mitigating the deleterious effects of fire on composite slabs. As such, they were designed to allow for testing in controlled lab conditions.

After construction, the pre-fire performance characteristics of the composite slabs were tested. Determining these performance characteristics required a mix of nondestructive and destructive tests. Nondestructive tests designed to assess skid resistance, surface hardness, and delamination from the substrate concrete were conducted across the entire surface of the larger composite slab and on the smaller slabs as well. Destructive performance tests designed to assess bond strength, rapid chloride penetration, abrasion resistance, and water penetration were carried out on cores collected at one end of the larger sized composite slab, and on specific smaller slabs set aside for testing the pre-fire exposure properties. These pre-fire tests were used as reference values for the condition of the slabs before exposure to a vehicle fire.

After the pre-fire tests, the larger composite slab was exposed to a realistic vehicle fire. Instrumentation of the composite slab and the vehicle with thermocouples allowed for the capturing of temperatures both within the vehicle and at different locations of the slab. Beyond the thermocouples used to capture the temperatures, heat flux sensors were also placed at two locations (behind and beside the vehicle) to

capture the heat flux from the vehicle, which will be representative of the exposure of surrounding infrastructure to the vehicle fire. This was planned to ensure that the test also captures some information on the effect of a vehicle fire on surrounding infrastructure.

Subsequently, after the vehicle fire test, similar tests were carried out under controlled conditions on the smaller sized slabs. These tests were done to replicate the thermal exposure of the larger slab, after the application of some fire-resistant materials as a protective layer over the PC surface. Performance tests similar to those used on the larger slab were then carried out to determine the effectiveness of the proposed protective coating in protecting the PC overlay from damage during fire exposure.

1.4 Outline of Report

The processes for carrying out these tests and the results from these tests are presented in subsequent sections. The next section (Section 2) lays out a review of the current state of the art in the use of PC and its design, alongside an analysis of vehicle fire accidents, previous vehicle fire tests, and fire department emergency response. In Sections 3, 4, and 5, the experiment designs are presented, including the design of the slab, its instrumentation, design of the test, instrumentation of the vehicle, and the planned performance tests to characterize the behavior of PC before and after vehicle fire exposure. Sections 6 and 7 present the results from the vehicle fire tests and the performance tests on the slab, respectively. Section 8 offers a proposed method for improving PC performance when exposed to elevated temperatures, and tests to delineate the effect of the proposed method. Section 9 offers concluding remarks, including limitations of the work and ideas for future work. The appendix shows results from the reliability tests of thermocouples in concrete cylinders, and tests on the validity of capturing delamination using infrared thermal imaging.

2. LITERATURE REVIEW

2.1 Application of PC on Bridge Decks as Overlays

The use of polymer concrete (PC) as an overlay material has gained popularity in recent years, due to its improved durability compared with traditional overlay materials. PC overlays are constructed to meet either AASHTO standards [9] or state authority specifications [5], and consist of a polymer adhesive and aggregate materials. Figure 2.1 shows the placement of PC as an overlay over a bridge deck. There are four main types of PC commonly used in overlays, each named for the principal adhesive used in them: epoxy polymer concrete, epoxy urethane polymer concrete, polyester polymer concrete, and methacrylate polymer concrete [10].

When used as overlays, PC performance is affected by several factors, including the mix design of the PC, the suitability of materials used, the integrity of the substrate structure, adequacy of surface preparation, compatibility between the overlay and the substrate, thickness of the overlay, bridge girder flexibility, environmental and traffic conditions, and quality of workmanship [11]. A particularly important factor in the performance of PC overlays is the mix design, with studies showing that the selection of materials and the ratio in which they are combined play a crucial role in the performance of the PC [12,13]. Two principal materials are used in PC, polymer adhesive and aggregate. The polymer adhesive usually consists of a base resin and an initiator. Together, these materials form the polymer adhesive, which acts as the binder. For the aggregates, several types are commonly used in PC. These are silica, quartz, granite, limestone, and basalt [14,15], and are required to meet some specific graduation requirements based on the conditions they are to be used in [14].

While PC offers many advantages as an overlay material, there are also some disadvantages acting as roadblocks to the widespread use of this material as overlays on road and bridge surfaces. Some of these shortcomings include the high cost of materials [16] and sensitivity of the resins to high temperatures, which lead to concerns about the material's ability to withstand exposure to elevated temperatures [17,18].

Studies into the effects of high temperatures on PC note that the presence of fire susceptible polymers in the concrete leads to adverse effects on the properties when exposed to elevated temperatures [19–22]. These studies determined that these elevated temperatures negatively impact both the short-term properties, such as compressive, tensile, and flexural strengths, and the long-term properties, with significant increases in creep deformation after exposure to high temperatures. They deemed that this loss of some of the most important characteristics of PC could be traced to the thermo-oxidative degradation of the polymer. Although limited, these studies expose an Achilles' heel of this otherwise excellent material, making it quite imperative to examine the behavior of this material as an overlay at elevated temperatures with the goal of devising solutions to improve its performance in such conditions.

Figure 2.1 Overlaying concrete bridge deck with polymer concrete [23]

2.2 Mix Design of PC

PC principally consists of the polymer resin, its initiator, and aggregates such as silica, quartz, granite, limestone, and basalt [13]. Other components such as fillers are added in as needed or to fulfill some specific requirement of the PC. The mix design process for PC closely parallels that of conventional concrete, involving the determination of the ideal proportions for each component. This approach enables the optimization of the mix design to achieve a balance between cost-effectiveness and performance enhancement [24]. By employing the absolute volume approach, Equation 1 illustrates the methodology for determining the mix design of a PC [24].

$$1.0 = \frac{P}{\gamma_P} + \frac{CA}{\gamma_{CA}} + \frac{FA}{\gamma_{FA}} + \frac{F}{\gamma_F} + Air \quad (1)$$

Where: P is the polymer weight, CA is the weight of coarse aggregate, FA is the weight of fine aggregate, F is the filler weight, and γ_P, γ_{CA}, γ_{FA}, and γ_F, represent the specific gravities of polymer, coarse aggregates, fine aggregates, and fillers, respectively.

Different studies on PC's mechanical properties have delved into determining the optimal mix design of PC that would optimize the properties under examination. This has led to a range of proposed ratios for the mix design of PC. Table 2.1 shows a selection of studies, the materials used, as well as the percentages of resin included in making the PC.

Table 2.1 reveals a diverse range of resin volumes tested across various studies, with these percentages contingent upon the specific resin type and the composition of the PC, including aggregates, additives, and fillers. Eventually, most investigations converged on an ideal polymer resin weight ranging from 12% to 15% of the total weight of the PC to achieve the optimal enhancement of the material's mechanical properties.

Table 2.1 Percentage content of resin in PC in different studies

Study	Resin	Additives/Fillers	Resin percentage
Niaki et al. [25]	Epoxy	Basalt fiber	25%
		Nanoclay	
Haurie et al. [26]	Epoxy	Magnesium hydroxide	20%
		Melamine polyphosphate	
		Ammonium polyphosphate	
		Hydromagnesite	
Tonet and Gorninski [27]	Polyester	Aluminum trihydrate	17%
		Polishing alumina residue	
		Fly ash	
Elalaoui et al. [28]	Epoxy resin	Aluminum trihydrate	6%–16%
		Ammonium polyphosphate	
Yasouj et al. [29]	Epoxy resin	Sodium alginate	13%
		Basalt fiber	
Golestaneh et al. [30]	Epoxy	Silica powder	10%–20%
Jafari et al. [31]	Epoxy		10%–14%
Muthukumar and Mohan, [32]	Furan	Silica powder	7.5%–15%
Ferdous et al. [33]	Epoxy	Fly ash	19%–45%
Seco et al. [34]	Polyester	Ladle slag	20%–45%
		Alumina	
Bulut and Sahin [35]	Polyester	E-plastic	10%–20%
Shokrieh et al. [36]	Epoxy	Glass fiber	10%–20%
Vipulanandan and Paul [37]	Polyester		10%–20%
Lokuge and Aravinthan [38]	Epoxy	Fly ash	20%–43%
	Polyester		
	Vinylester		

2.2.1 Advantages and Disadvantages of PC on Bridge Decks as Overlays

Using PC as an overlay material has several advantages. This material has mechanical properties that greatly exceed those of other overlay materials. Also, PC can be effective even when applied in very thin layers (even as low as ¼-inch thick). With such thin profiles, surfaces finished with PC overlays may not require modifications to other infrastructure such as median barriers, guardrails, signposts, or drainage structures, and clearance problems are easily avoided. Furthermore, using such thin layers ensures that the overlays' relatively light weight minimizes the added dead load on bridge structures [39, 40]. PC also offers high protection against moisture and chloride ion ingress [40–43] and is resistant to acids and petroleum products [44]. This material also achieves high early strength and cures rapidly, typically able to withstand traffic loads within two hours of placement [44–46], thus minimizes the time a road needs to be closed to traffic. In addition, PC can be placed in variable thicknesses, making it a useful material for making profile corrections to improve ride quality when used as overlay. PC also has long service life, with the overlays generally expected to offer adequate protection to bridge decks for up to 20 years [42, 43, 46].

While PC offers many advantages as an overlay material, it also has several disadvantages that should be carefully considered. These include the high cost of materials [16], emission of noxious odors from the fresh mix, short working life of the binder (between 10 and 60 minutes), flammability of the resin and

primer [17], which could lead to increased risks of fire outbreaks during construction, and sensitivity to elevated temperatures. These materials' high sensitivity to elevated temperatures has led to concerns that a vehicle fire may degrade or even completely destroy a PC overlay on a bridge deck. Also, the deformation incompatibility between PC and concrete usually used as substrate (PC typically has a thermal coefficient of expansion two to three times higher than that of concrete [6, 7]) may lead to loss of bond and extensive damage.

2.2.2 Performance of Polymer Concrete at High Temperature

The performance of PC under elevated temperatures is a crucial consideration for structural safety, significantly influencing its applicability in construction and other occupied structures. Generally, polymers initiate or spread fires because, being organic compounds, they decompose into volatile products on exposure to heat. Thus, a primary drawback associated with employing PC in structural and residential buildings is its susceptibility to fire, given its classification as a material with medium to high flammability [47].

Thermoset polymers are commonly used as PC binders [24, 48]. Thermoset polymers, characterized by their cross-linked molecular structure, generally offer superior thermal stability compared with thermoplastics. Nevertheless, even thermoset polymers are not impervious to the effects of high temperatures. Thermal decomposition, a chemical process in which a substance breaks down into simpler compounds or elements due to heat exposure, can occur.

Extended exposure to temperatures exceeding their thermal stability thresholds can result in degradation, manifesting as alterations in mechanical properties, discoloration, and potentially the formation of char. During the pyrolysis process, wherein the polymer resins within the PC undergo high-temperature decomposition, voids or pore spaces emerge within the material, causing a disruption in the bonding between the resin and the aggregates. Consequently, this phenomenon results in a decrease in the material's desirable properties. An examination of the response of methacrylate-based PC and polyester-based PC to elevated temperatures revealed discernible weight loss in both PC formulations, as documented by [49]. Specifically, the methacrylate PC exhibited substantial weight reduction beyond 315°C for two minutes and 271°C for 10 minutes, and a similar pattern was observed with the polyester PC, which displayed analogous trends when exposed to temperatures exceeding 327°C for two minutes or 282°C for 10 minutes.

The PC response to elevated temperatures is closely tied to a crucial property known as the heat distortion temperature (HDT). The HDT represents the temperature at which a solid material starts to deform or lose its structural integrity under specific loads or stresses. This parameter is of paramount importance for evaluating the heat resistance and dimensional stability of a wide range of materials, including polymers and plastics.

Several studies have explored how changes in mechanical properties occur in PC when exposed to elevated temperatures. Notably, these investigations have established a direct correlation between the mechanical properties of epoxy PC and polyester PC and the HDT values of the polymer resins employed [50, 51]. This connection is attributed to the fact that the HDT values of these polymer resins are lower than their respective glass transition temperatures [50]. Consequently, once the temperature surpasses the HDT of the resin, the mechanical strength of the PC diminishes rapidly [50, 51].

Various strategies have been investigated to enhance the resilience of PC against thermal influences, each with a range of success. These tactics encompass the incorporation of flame retardants, reinforcement with fibers, utilization of nanofillers, and the application of intumescent coatings, each operating through distinct mechanisms such as char formation, flame suppression, heat absorption, barrier establishment, and improvement of thermal conductivity. The selection of a particular strategy hinges on the unique demands

and factors relevant to the application at hand, encompassing criteria such as fire performance, environmental considerations, and cost-effectiveness.

2.2.3 Improvement of the Fire Resistance of PC

Several methods have been investigated to improve the fire resistance of PC. These methods involve either the addition of other materials into the mix to enhance the fire resistance of the PC, or a targeted use of a fire resistance intumescent coating to limit exposure of PC when used in practice.

2.2.4 Enhancement of Fire Resistance of PC

The most commonly used approach to improving PC's fire resistance is the addition of other materials beyond the basic constituent materials into the PC mix. These materials could be added as fiber reinforcement or nanofillers [25, 29]. Such materials, while not usually added to PC to improve its fire resistance, have been shown to do so nonetheless without having a detrimental effect on the mechanical properties of PC [25, 29].

Fiber reinforcement has been known to improve some mechanical qualities of concrete such as its strength. With this knowledge, some studies [25, 29] theorized that the use of this material could also lead to improvements in PC fire resistance by improving the material's structural integrity at high temperatures, enhancing its resistance to thermal cracking and providing additional strength during fire events. To this end, some studies [25, 29] have investigated the use of basalt fibers, to reinforce the resistance of PC to elevated temperatures. The results from these studies showed this to be a promising method, albeit with some caveats as improvements in the properties are dependent on the type of fiber used and its distribution within the PC. In addition, the use of fiber reinforcement in PC increases the cost of what is an already expensive material.

The incorporation of both inorganic fillers, such as micro-silica or nanoparticles, as well as nano-clays into PC has been explored to enhance its fire resistance. These studies [25, 52, 53] have investigated the effects of incorporating inorganic fillers on the fire behavior of PC and shown that these fillers can enhance the material's thermal stability, increase its char formation, and provide a barrier against heat transfer during fire exposure. In addition, the use of nanofillers offers some improvements to the mechanical properties of PC. However, these materials also lead to increases in the PC's material density and weight; also, the improvements to fire resistance from using these materials has been relatively minimal. In addition, the long-term behavior and potential health/environmental impacts of nanoparticles remain unknown and require further investigation.

An alternative approach directly targeted to improve PC fire resistance is the incorporation of flame-retardant additives [26–28]. These additives include halogen-based compounds, phosphorus-based additives, and aluminum-based additives, each of which works with different mechanisms to improve PC fire resistance. Halogen-based additives, like brominated compounds, enhance the PC's fire resistance through the mechanism of flame inhibition, displacing oxygen by producing gases to suffocate the fire. When exposed to fire, these additives release bromine radicals, which interrupt the combustion process. The bromine radicals combine with the active radicals generated during combustion, thus disrupting the chain reactions involved in the combustion process. This interruption reduces the flammability and heat release of the PC, leading to improved fire resistance. Phosphorus-based additives, such as ammonium polyphosphate (APP) and red phosphorus, improve the fire resistance of PC through two mechanisms. During fire exposure, these additives undergo thermal decomposition and release phosphoric acid. The phosphoric acid acts as a flame retardant by forming a protective char layer on the surface of the material. This char layer acts as a barrier, reducing the access of oxygen to the combustible components and inhibiting the spread of flames. Also, the gases release displace oxygen helping to suffocate the fire. Aluminum-based additives, such as aluminum hydroxide and aluminum trihydrate, improve PC fire

resistance through their endothermic and char-forming properties. During fire exposure, these additives release water vapor due to their relatively high water content. The water vapor absorbs heat from the surroundings, which helps to cool down the material and delay its temperature rise. Additionally, the decomposition of aluminum hydroxide and aluminum trihydrate releases inert gases, further diluting the flammable gases and reducing the flammability. These additives also promote the formation of a protective layer of alumina (Al_2O_3), which acts as a heat barrier and prevents further heat transfer to the underlying material [27, 28].

The use of flame-resistant additives in PC has some advantages. These include effectively reducing the flammability and heat release rate of the PC, and ease of use. However, the introduction of these materials into PC also has some downsides. Some fire-resistant materials contain halogens, which break down into harmful chemicals such as dioxins when they burn, and thus pose a risk to human health and the environment [54]. Also, some studies into the effects of fire-retardant additives on the mechanical properties of PC have shown that adding some of these additives leads to a reduction in the mechanical properties at ambient temperature [26, 29]. The formulation and concentration of the additives could also have an adverse effect on the properties.

Several studies have investigated the use of these fire-retardant materials in PC and their attendant effects on the fire resistance [25–29]. These studies covered two of the principal types of polymer resins used in PC (epoxy polymer resin and polyester polymer resin), used in varying mix ratios with aggregates and some additives. Utilizing a range of mechanical tests and varying conditions, the studies showed that these additives could improve both the residual mechanical properties (properties after the material has returned to ambient temperatures), and the properties at high temperatures. However, the results also indicate that the effect of these additives is limited; beyond 250ºC–300ºC they lose their insulative abilities and the PC starts degrading quickly.

2.2.5 Protection of the PC Using an Intumescent Coating

Intumescent coatings have been studied as a method to enhance PC fire resistance. Intumescent coatings are usually a blend of materials that form a protective char layer when exposed to fire, insulating the underlying material and delaying its thermal degradation. The material constituents of intumescent coatings are usually selected to retard fires and temperatures from the underlying materials by swelling to produce a thermally insulative char, removing heat via endothermic reactions, and displacing oxygen by producing gases to suffocate the fire. A study focused on the development of intumescent coatings showed that a blend of materials such as graphene and graphene oxide additives, which expand upon exposure to heat, and other flame-retardant materials (halogen-based or aluminum-based) to polymer resins to form intumescent coatings that can adhere to most surfaces, could create a viable intumescent material with good adhesion for use in protecting surfaces from the effects of fire [53]. These additives form a highly thermally conductive network within the polymer matrix. During fire exposure, this network facilitates the efficient dissipation of heat, preventing localized overheating and reducing the spread of flames [53]. Intumescent coatings have a number of advantages, especially their applicability for retrofitting existing structures, as they are applied as surface coatings, and their versatility, as they can be designed with specific flame-retardant mechanisms in mind. However, these coatings could require periodic maintenance, and their application may further increase the cost of PC, compared with directly introducing fire resistant materials directly into the PC mix.

In summary, from the examination of existing studies, the aim of improving PC fire resistance presents a multifaceted challenge, and while various approaches have been explored, there is no universal remedy that suits all scenarios. When dealing with freshly mixed PC, one potential avenue for enhancing its fire resistance involves the incorporation of fire-retardant materials, either individually or as a combination of different materials, each offering complementary mechanisms to dissipate heat and restrict temperature

increases. However, this method comes with a caveat; it may inadvertently alter the mechanical properties of PC, potentially compromising some of its more desirable attributes. Moreover, this approach is not applicable to existing PC applications, limiting its practicality. For scenarios involving existing PC applications, an attractive alternative is the introduction of an intumescent layer. This solution is particularly well-suited for retrofitting and could even be applied as a finishing layer during construction without significantly altering the core properties of the PC mixture. However, it is essential to acknowledge that implementing an intumescent layer can entail additional costs, which can be significant considering that PC is already an expensive construction material. Therefore, it becomes imperative to carefully evaluate the distinct needs and constraints of each specific situation before deciding on the most suitable approach to enhance PC's fire resistance.

2.3 Vehicle Fire

2.3.1 Statistics Summary of Vehicle Fire Accidents

According to the U.S. Fire Administration's (USFA) National Fire Incident Reporting System (NFIRS) from 2014 to 2016, the majority of highway vehicle fires (66%), occurred in passenger vehicles [55]. A survey carried out by the National Fire Protection Association (NFPA) showed that there are three principal causes of vehicle fires: mechanical failure, electrical failure, and collision. Fires resulting from mechanical failures constitute the majority (58%), and those from collisions constitute the least (3%) [56]. The National Automotive Sampling System (NASS) database [57] shows that a majority of collisions leading to vehicle fires were front ended. These led to fires initiated in the engine compartment. For rear and side collisions and rollovers, fires were commonly initiated in the rear end, interior, in pooled flammable liquids under the passenger compartment, and by hot exhaust systems. From studies by [58], it was determined that vehicle fires from rear-end collisions spread more rapidly, making this a very critical scenario when studying highway vehicle fires, especially when factoring in the response times of fire departments.

2.3.2 Emergency Response Time of Fire Departments

An important variable in understanding the response of PC surfaces to elevated temperatures from fires is the exposure time. This is dependent on the spread of vehicle fires and time of burn. NFPA 1710: Standard for the Organization and Deployment of Fire Suppression Operations, Emergency Medical Operations, and Special Operations to the Public by Career Fire Departments establishes the criteria for emergency response to fire. This standard prescribes that the first engines should arrive at a fire scene within 240 seconds of a call being made for 90% of fire incidences [59]. However, one study [60] analyzed 13,463 daytime fire response records and 2,681 recorded nighttime responses and found that fire departments' emergency response time is usually between seven and eight minutes, including travel time. Figure 2.2 shows the response time relating this to the heat release rate for vehicle fires ignited by gasoline leakage.

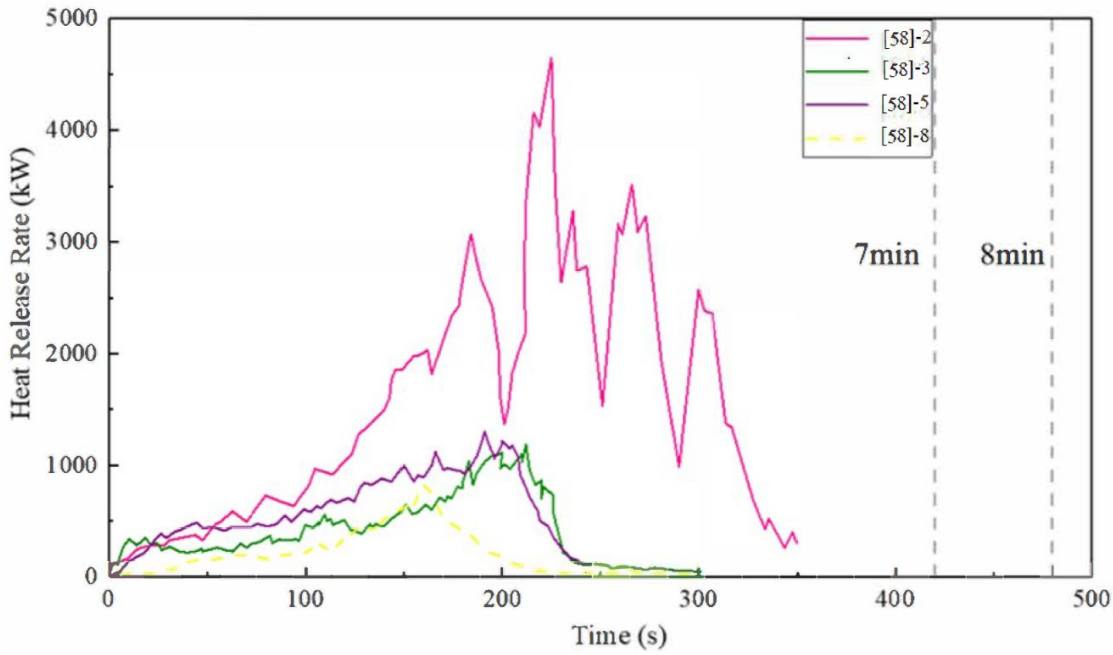

Figure 2.2 Fire departments' emergency response time compared with heat release rates from experiment

2.3.3 Previous Vehicle Fire Tests

In recent years, more and more scholars have paid attention to full-scale vehicle fire tests in a bid to better understand the causes and the process of propagation of such fires. Between 2001 and 2003, Tewarson et al, [58] performed fire tests on seven types of vehicles subjected to different crash conditions in order to study and document the fire propagation behavior. Other studies carried out fire tests on a variety of vehicles to collect data on the burning behavior and fire spread characteristics of the vehicles [23, 61–64]. Table 2.2 gives an overview of previous vehicle fire tests.

Table 2.2 Vehicle model, fuel, and ignition position for different tests

Author	Year	Vehicle	Fuel	Ignition position	Ref. No.
Jeffrey Santrock	2001-2003	Dodge Caravan (1996s)	Engine compartment fluids	The battery and the power distribution center	[58]-1
		Plymouth Voyager (1996s)	243 ML/min fuel tank leak ignited at 32s.	Under vehicle	[58]-2
		Chevrolet Camaro (1997s)	515 ML/min fuel tank leak ignited at 31s.	Under vehicle	[58]-3
			A mixture of 3 quarts of automatic transmission fluid	Right side of the engine compartment	[58]-4
		Ford Explorer (1998s)	750 ML/min fuel tank leak ignited at 30s.	Under vehicle	[58]-5
			350 ML/min fuel tank leak ignited at 30s.	Under vehicle (mid-body)	[58]-6
		Honda Accord (1998s)	2 liters of a 1:1 mixture of antifreeze and water	The windshield washing fluid	[58]-7
			400 ML/min fuel tank	Under vehicle	[58]-8

Author	Year	Vehicle	Fuel	Ignition position	Ref. No.
			leak ignited at 35s.		
		Chevrolet Camaro (1999s)- - standard plastic parts	Engine compartment fluids	Engine compartment	[58]-9
		Chevrolet Camaro (1999s)- containing fire retarded polypropylene	Engine compartment fluids	Engine compartment	[58]-10
		Ford Explorer (1999s) --standard plastic parts	300 ML/min fuel tank leak ignited at 30s.	Under vehicle	[58]-11
		Ford Explorer (1999s)- containing an intumescent paint	Engine compartment fluids	Left side of the engine compartment	[58]-12
Katsuhiro Okamoto	2009	Sedan passenger car (1990s)	10L	Right rear wheel	[61]-1
			10L	Right rear wheel	[61]-2
			20L	Right rear wheel	[61]-3
			10L	Left front seat	[61]-4
	2013	Minivans (1990s)	10L	Right rear wheel	[23]-1
			10L	Right side of the front bumper	[23]-2
			10L	2nd row seat in the passenger compartment	[23]-3
			10L	Back row seat in the passenger compartment	[23]-4
Xuan Sun	2010	Audi A6 (1997s)	20L	The rear seats	[62]
Xiaohui Jiang	2018	Volkswagen's saloon	Very little gasoline (<1%)	Engine compartment	[63]
Hui Zhu	2020	Sedan vehicle	the fuel tank was filled with water	Engine compartment	[64]

From Table 2.2, note that the different tests were carried out under varying conditions and targeted fires starting in different locations of the vehicles. Figure 2.3 shows the resulting heat release rates (HRR) for the different tests, and Figure 2.4 shows the maximum temperatures reached in the tests.

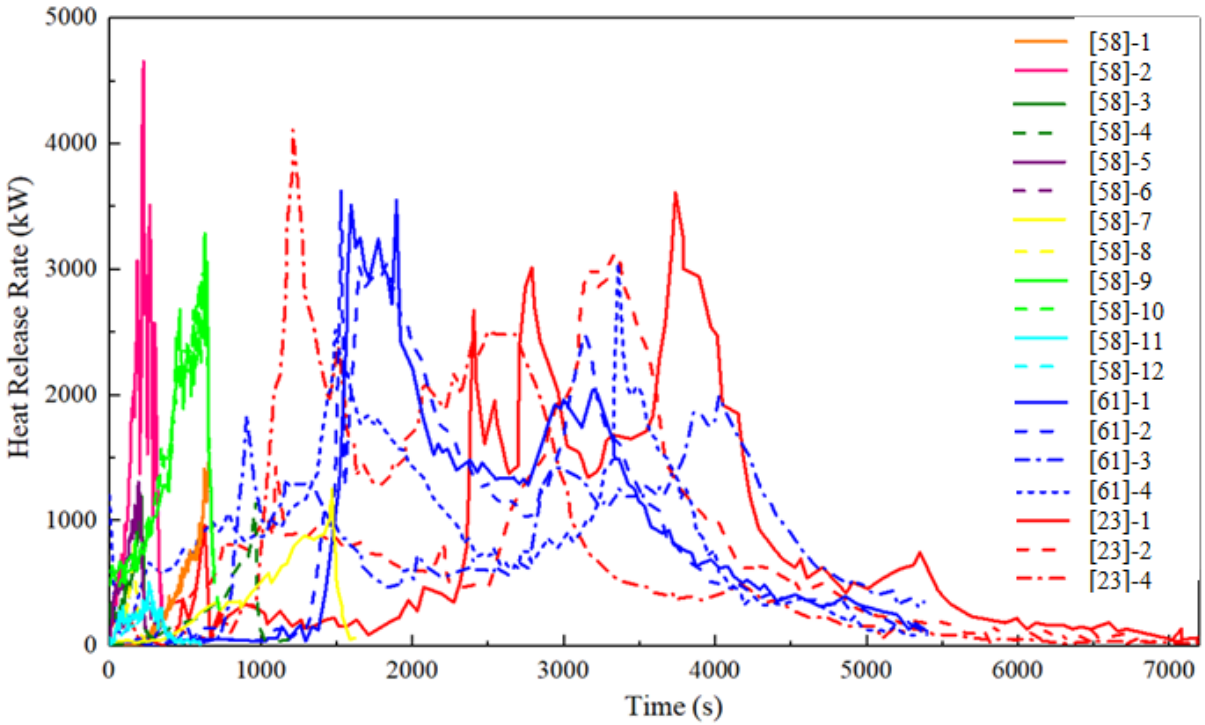

Figure 2.3 HRR curves in references [23, 58, 61]

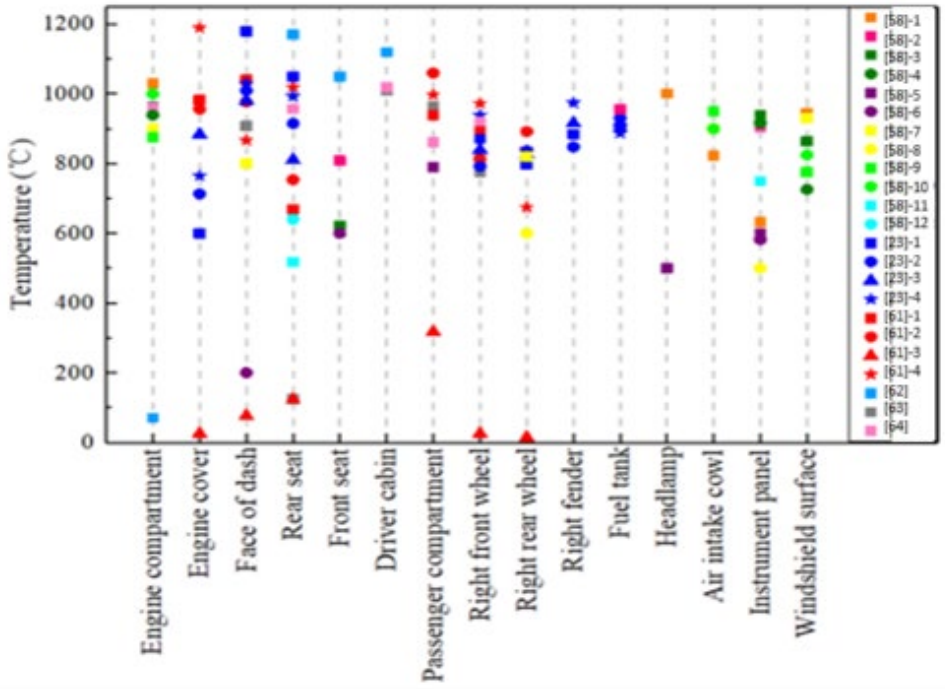

Figure 2.4 Temperature at different locations [23, 58, 61–64]

From the plots in Figure 2.3, two distinct sets of patterns can be noted. The first for short duration fires (under 1,000s), and the second for much longer fires. In the short duration tests, the fires were suppressed after a predetermined interval, while in the second set, the fires were allowed to run their full course. Although influencing the heat release patterns, the length of the fires did not seem to affect the maximum

HRR. Rather, the HRR seems to be a function of the parts of the vehicle that caught fire. Curve 2 from [58], which showed the highest HRR of about 4,700 kW, was ignited by gasoline leaking out of the vehicle under the gas tank, creating a flammable pool beneath the vehicle. In this test, the flames spread rapidly, and the fire reached the maximum HRR in about 260s. Manual suppression meant that the fire was also quickly put out, with the whole test lasting under 300s. Similarly, curve 9, also from [58], started by igniting the engine compartment fluids, reached a maximum HRR of 3,300 kW at about 780s, at which time it was quickly suppressed. The HRR in other short duration tests did not reach these heights. For the longer duration fires, the trends show similarities to the shorter duration fires except with multiple peaks and lasting for longer periods. With the burning regimen lasting much longer than the short duration tests, these tests had distinct periods where different ignitable fluids caught on fire, and thus developed multiple HRR peaks congruent to these time instances.

From Figure 2.4, it can be noted that the temperatures in different locations for the same vehicle fire tests differ significantly. In addition, the maximum temperatures for different vehicle fire tests in the same locations also has some dispersion. Both can be attributed to flammability of materials encountered by the flames. Some areas of the vehicle such as the engine compartment and areas close to the gas tank are exposed to fires which give off more heat, and thus record higher temperatures than areas with less flammable materials. The maximum temperature recorded in these tests was close to 1200^{o}C. These tests indicate that irrespective of duration, highway/bridge surfaces exposed to vehicle fires can be exposed to temperatures exceeding 1000^{o}C, and thus, an experimental vehicle fire carried out to determine the behavior of overlay materials, needs to attain such temperatures.

3. DESIGN AND CONSTRUCTION OF THE TEST REINFORCED CONCRETE PANEL

Simulating a vehicle fire on a PC overlaid concrete bridge deck requires the design and construction of a slab replicating a bridge deck with finished with a PC overlay. This design entailed the use of design parameters and materials as approved by relevant authorities from whom approval of materials and design for transportation infrastructure is necessary. Furthermore, to capture the exposure of the slab to heat from the vehicle fire, thermocouples were used to instrument the slab at uniformly distributed positions over the surface and in the interface between the PC overlay and the substrate concrete. This was designed to allow for a characterization of the heat exposure across the surface and through the cross section of the PC overlay. The design and construction of the slab and its instrumentation are described below.

3.1 Design and Construction of the Concrete Panel

In the vehicle fire test, the composite panel was cast on the ground directly. According to the Structures Design and Detailing Manual from Utah Department of Transportation 16.2.3 [8], the minimum thickness for a bridge deck should be 8 inches, and the minimum reinforcement size should be #4 steel. The top and bottom transverse reinforcement are required to be offset, preferably at half of the spacing, spacing of steel should not exceed 18 inches, and reinforcing steel needs to be Grade 60 or better. A minimum top cover of 2.5 inches and bottom cover of 1 inch are also recommended [8].

Keeping in accordance with all the stated requirements, a slab of 36 ft (length) x 20 ft (width) x 8 inch (thickness) was constructed, reinforced using #4 grade 60 steel, placed at 6 inches spacing for the top and 8 inches spacing for the bottom layer. The clear cover thicknesses were 2.5 inches and 1 inch for the top and bottom, respectively. The cover thickness for both short sides was 2 inches, while on the longer side, a 4 ft unreinforced section was added to one side to use for core sampling of the slab prior to carrying out the vehicle fire tests, bringing the total length of the panel to 40 ft.

The concrete used in casting the slab is class AAA concrete with compressive strength of 4.5 ksi. The overlay is made of a polyester polymer concrete (PPC) mix. This PPC mix is laid over the concrete to an average thickness of about 1 inch. The PC consists principally of a polymer resin, and aggregate. To perfect the bond of the PC to the concrete substrate, a resin primer is applied to the surface prior to laying the concrete. High molecular weight metacrylate (HMWM) resin primer is used for this purpose. In addition to ensuring a strong bond between the overlay and substrate concrete, this primer also acts as a sealer to seal up any existing cracks in the substrate concrete prior to the overlay being placed [65]. The last material used is the finishing sand. Commercial quality blast sand is used for this purpose, with at least 95% passing through the No. 20 sieve and having a maximum absorption of 1%.

The layout of reinforcement is shown in Figures 3.1 to 3.3. Figure 3.1 shows the plan view of the reinforcement layout, while Figures 3.2 and 3.3 show the cross-section view of the reinforcements for the 20 ft and 36 ft directions, respectively. Call outs are used to offer a detailed view of the reinforcements in both cross-section figures. Figure 3.4 shows the various stages of the construction process for the concrete slab.

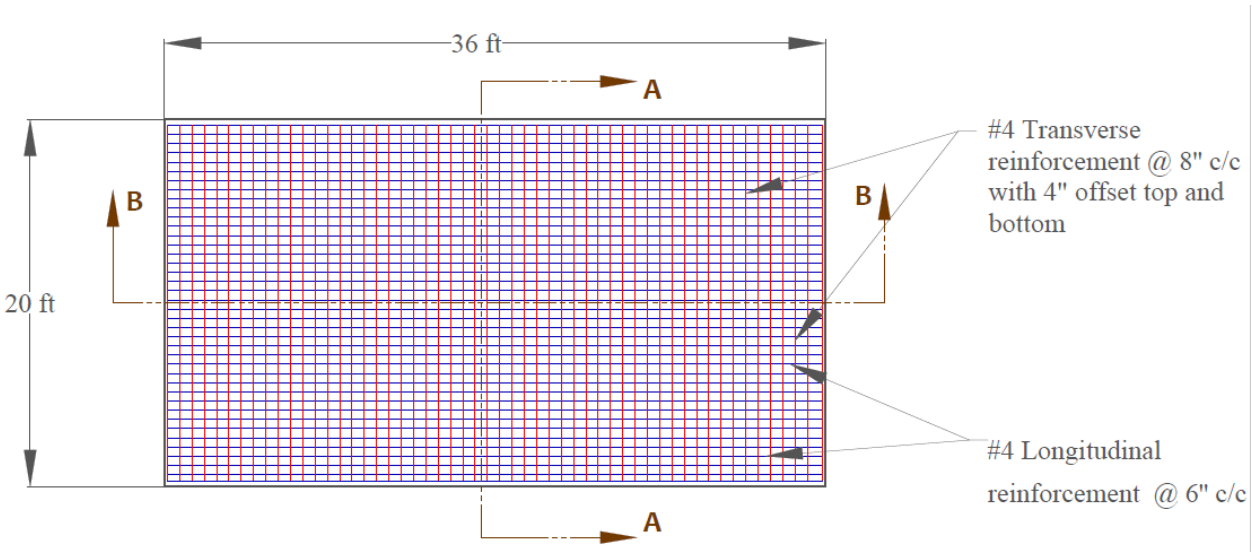

Figure 3.1 Layout of the reinforcement

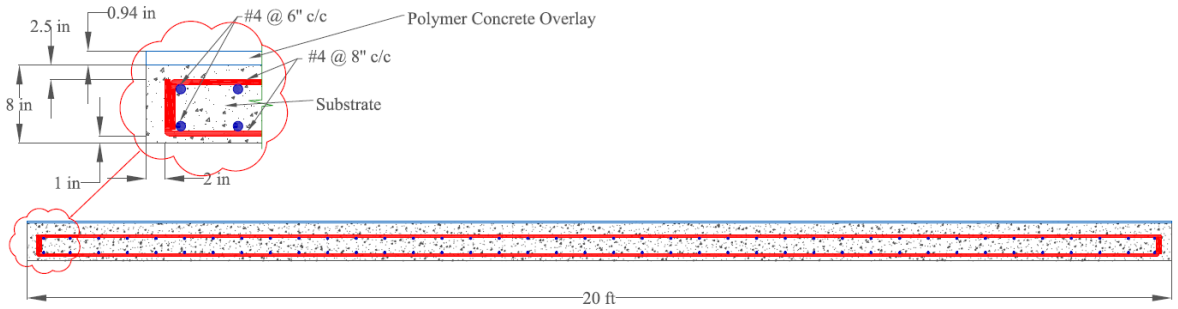

Figure 3.2 Section A-A

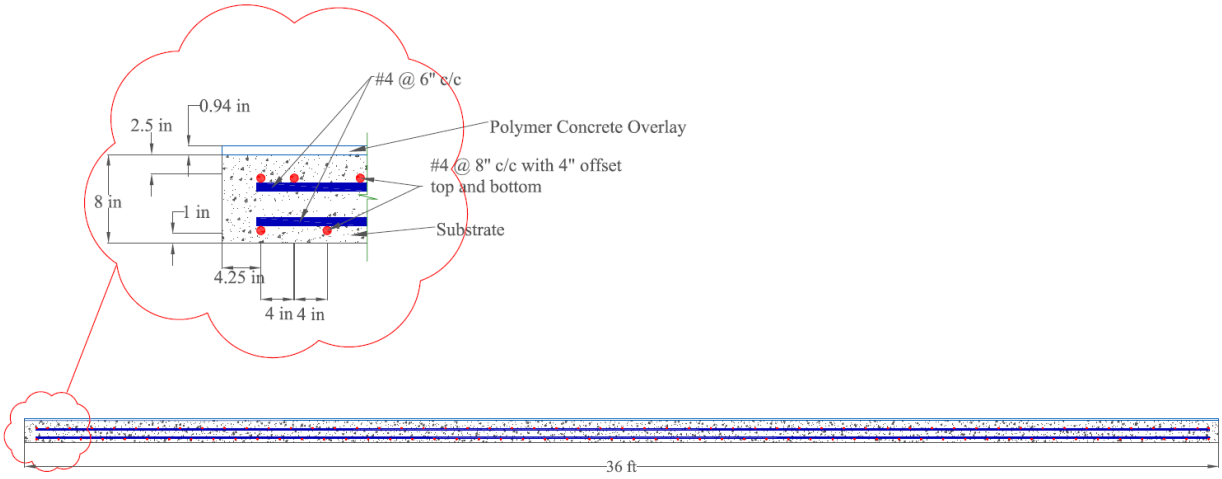

Figure 3.3 Section A-A

(a)

(b)

(c)

Figure 3.4 a) Rebar placement for the slab b) pouring the concrete and c) the finished concrete after pouring

3.2 Overlay Materials

The PC overlay to be used over the concrete deck consists of PPC 1121, obtained from Kwik Bond polymers. This resin and its hardener (methyl ketone peroxide), mixed with aggregate, constitute the principal components of the PC. As per UDOT specifications, the PC was planned to be laid to a thickness of under 1 inch [5,65]. This overlay is bonded to the concrete deck using a high molecular weight metacrylate (HMWM) resin primer and the surface finished off using finishing sand.

The selected resin meets a number of specifications of physical properties as can be found in the UDOT specifications for thin bonded overlays [5,65]. These properties include a minimum compressive strength of 5,000 psi, a minimum tensile strength of 2,000 psi, tensile elongation between 30% and 80%, maximum water absorption of 1%, shore D hardness between 60 and 75, gel time of between 15 and 45 minutes, 100% adhesion to concrete, and a flexural yield strength of 3,000 psi. According to UDOT specifications, the resin content of the PC must be 12% (±1%) by weight of the dry aggregate used in the concrete [65].

Two types of aggregate are commonly used in PC: basalt aggregate and calcinated bauxite aggregate. When used in overlaying a deck, these aggregate types need to meet some specific requirements, including specific gradation, maximum moisture content of 0.2% by weight, magnesium sulfate soundness of 15% maximum, and LA abrasion grade D of 20% maximum. Some other requirements, which are specific to the type of aggregate, include the micro-deval abrasion, which is 10% maximum for basalt and 5% maximum for calcinated bauxite, and Moh's scale hardness of 7 minimum for basalt and 8 minimum for calcinated bauxite.

To perfect the bond of the PC to the concrete substrate, a high molecular weight metacrylate (HMWM) resin primer is applied to the surface prior to laying the concrete. In addition to ensuring a strong bond between the overlay and substrate concrete, this primer also acts as a sealer to seal up any existing cracks in the substrate concrete prior to the overlay being placed [65]. According to UDOT specifications, the selected primer has low odor and no wax content, has a maximum volatile content of 30%, viscosity of 25 cP, specific gravity of 0.9, minimum dry bond strength of 700 psi after 24 hours, maximum vapor pressure of 0.039 in. Hg, and a minimum flash point of 180ºF.

The last material used in a PC overlay system is the finishing sand, which is important for improving the skid resistance of the overlay. Commercial quality blast sand, with at least 95% passing through the No. 20 sieve and having a maximum absorption of 1%, was used for this purpose.

3.3 Casting the PC

Prior to application of the overlay, the substrate concrete panel was allowed to cure for at least 28 days. After curing, the concrete surface was kept dry for 24 hours prior to placing the overlay. Application was planned to take place with the dry surface at temperatures of between 50ºF and 90ºF. Prior to application of the PC, the surface was prepared by shot blasting of the concrete to remove impurities and create a good bonding surface for the overlay. The surface of the concrete was then cleaned using compressed air to remove any loose materials on it.

The HMWM resin primer was first mixed and applied uniformly to the concrete surface immediately after mixing. Next, the polyester resin and hardener were blended. This was then mixed with the aggregate in a mixer until uniform in texture and appearance. This mix was then poured onto the prepared concrete slab after 15 minutes from the time of the HMWM resin primer application.

After leveling off the PC surface, finishing sand was then applied over the PC before initial set of the overlay. After applying the finishing sand, the PC was then allowed to cure for at least four hours before further work could be done on it. Figure 3.5 shows the various stages in laying the PC overlay on the concrete slab.

(a)

(b)

(c)

Figure 3.5 Construction of polyester polymer concrete overlay a) preparing the surface using grinders, b) pouring the HMWM primer, and c) pouring the PC

3.4 Instrumentation of the Concrete Panel

One of the most important parameters to be captured during the fire test is the temperature at different locations through the cross-section of the deck. To measure these temperatures during the test, thermocouples were installed at two locations on the constructed slab. These were on the surface of the slab and at the interface between the PC overlay and substrate concrete. The thermocouples on the surface were made of type K 20-gauge thermocouple wires with ceramic fiber braid insulation, which can resist temperatures up to 1,427ºC. These thermocouples were designed to withstand high temperatures and accurately measure the surface temperature of the panel during the test. The thermocouples at the interface were made of type K 24-gauge wires with fiberglass insulation, rated for temperatures up to 482ºC. These thermocouples were used to measure the temperature at the interface between the PC overlay and substrate concrete, which is a crucial area to monitor during the test as it is an area where delamination may occur if the temperature exceeds a certain limit. Thermocouples were not placed below the interface as it was expected that temperatures would not increase significantly in that area during the short duration of the fire test. The thermocouples at the interface were laid along the top rebar with only the beaded end extending beyond the concrete cover to avoid inducing delamination by having the wires lying along the interface. Table 3.1 shows the properties of the different thermocouples used.

The thermocouples were made by stripping both wires, twisting them together and then welding the end of the twisted section using a thermocouple welder. This was to ensure that the contact between both wires, which creates a thermocouple sensor, remains secure.

The thermocouples were distributed evenly across the panel. This placement was done to ensure that the thermal exposure of the panel surface and substrate concrete were adequately captured. Additional thermocouples were placed near the side closest to the gas tank, where temperatures were expected to possibly be significantly higher than elsewhere on the panel. Thus, collecting more temperatures in this region proved useful for analyzing the effects of the temperature on the panel. Figure 3.6 shows the position of the thermocouples across the surface of the panel. Each thermocouple wire was extended at least 15 feet beyond the edge of the panel for safety to ensure that all personnel and equipment used in collecting the data stayed at a safe distance from the fire. Table 3.1 shows the different types, location, and quantity of sensors used in the experiment.

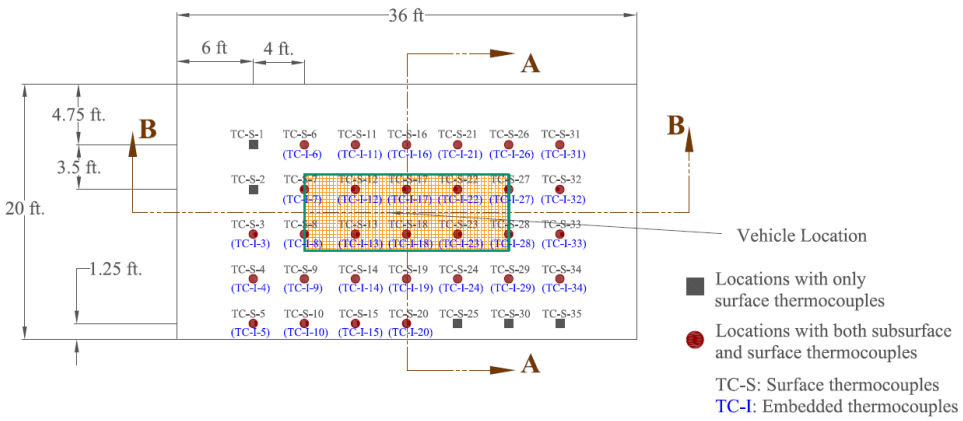

Figure 3.6 Layout of thermocouple sensors at both the surface of the overlay and at the interface between the overlay and concrete

Table 3.1 Different types, location, and quantity of sensors used

ID	Sensor type	Model	location	No.
A	Thermocouple	TYPE-K 20-gauge, high temperature fiberglass braid	Interface between concrete substrate and overlay	30
B	Thermocouple	TYPE-K 20-gauge, Ceramic fiber braid	On concrete surface	35

Several data acquisition systems from Campbell Scientific Inc. (CR 1000, CR1000X and CR3000) were used to collect the temperatures over the test duration. The data acquisition frequency was set to 1s, thus meaning a temperature and heat flux was recorded from each thermocouple and heat flux sensor every second over the duration of the test. An example of a data acquisition system is shown in Figure 3.7.

Figure 3.7 CR3000 Data Acquisition System

4. DESIGN OF THE VEHICLE FIRE TEST

The experiment was designed to simulate a car catching fire alone on the highway. To simulate the real vehicle fire accident, the experiment was planned for outdoors. The vehicle fire involved two critical components: elevated temperatures on the overlay and slab, and heat flux to surroundings. Both are produced as the fire progresses through the different parts of the vehicle, and it was expected that there would be changes in each as the fire progressed depending on the combustibility of different parts of the vehicle. The test vehicle and instrumentation placed to capture these effects are described below.

4.1 Description of the Test Vehicle

The vehicle tested in the fire was a 2007 Subaru Outback, as shown in Figure 4.1. This is an all-wheel drive, gas powered four-cylinder vehicle. All the auto parts and interior decoration and components were kept intact before the experiment. The interior of the vehicle was made of fabric and fiberglass, and the fuel tank holds 15.9 gallons when full. The configuration parameters of the experimental vehicle are shown in Table 4.1. Figure 4.2 shows the placement of the vehicle on the slab.

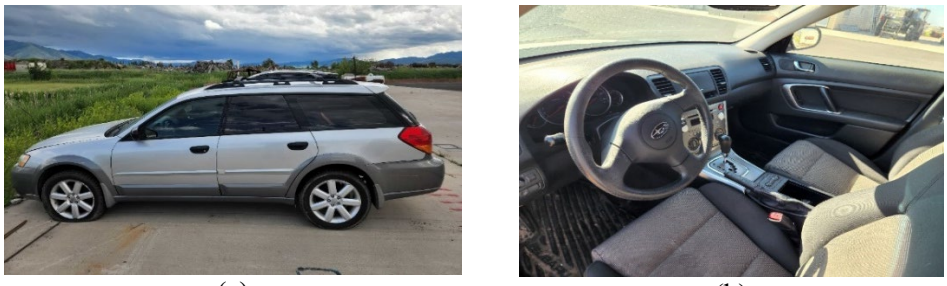

(a) (b)

Figure 4.1 2007 Subaru outback (a) exterior appearance and (b) interior

Table 4.1 The configuration parameters of 2007 Subaru Outback

Type	Configuration parameters
Drive Type	All-wheel drive
Engine	gas 4-Cyl 2.L/150 vehicle
Fuel Tank Capacity	15.9 gal.
Gross Weight	4,325 to 4,635 lbs.
Dimension	186”–189” L x 68” –70” W x 56” –62” H
Exterior Colors	silver
Finish of seats	fabric
Finish of center console	leather

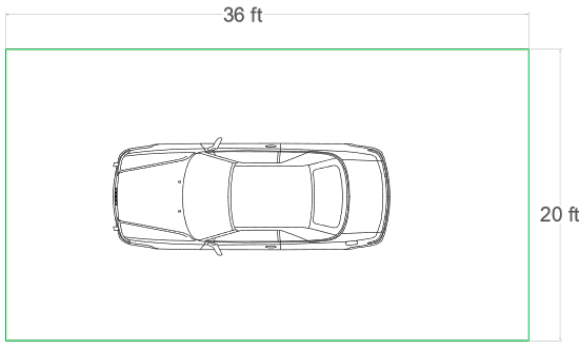

Figure 4.2 Simplistic view of fire test for polymer concrete overlay over bridge deck

From a literature review, including tests on vehicle fires and expected response times of firefighting services, some testing parameters were determined. It was decided that the fire would be a simulation of a vehicle fire triggered from a leak in the gas tank after a rear-end collision. To replicate experiments designed to simulate fires started in this manner, a 3-mm diameter hole was drilled in the bottom of the fuel tank close to the right rear wheel and plugged up [58]. To simulate the fuel tank leakage after the collision, the process of the experiment began with adding 2.4 gallons of gasoline to the fuel tank. The small amount of gasoline represented a vehicle that has been in use and had a relatively small amount of gas left in the tank. The plug was then removed from the hole at the bottom of the fuel tank, and gasoline was allowed to flow out of the hole drilled into the tank onto the ground. After 90 seconds, gasoline spilled onto the ground was ignited by a hand-held flare, the fire was allowed to burn, and then eventually put out by firefighters. To simulate the condition of the vehicle after a rear-end crash, the rear windshield was broken, both rear windows opened, the trunk windows broken, and the driver's and left passenger's doors were slightly ajar, as shown in Figure 4.3.

(a) (b)

Figure 4.3 The state of the vehicle before the test: a) rear windshield and left rear and trunk windows broken, and driver's door open, and left passenger door ajar; and b) right rear and trunk windows broken

As the oils, such as engine, transmission, and brake oil, in engine compartment can affect how quickly the fire spreads, actual car fires may spread faster than fires in scrapped cars [73]. Thus, all oil in the engine compartment is retained during the experiment.

4.2 Instrument of the Vehicle

To measure temperatures within the vehicle during the test, thermocouples were placed at different locations. These thermocouples were intended to capture the temperature changes at different locations during the fire. The thermocouples used in the vehicle were made of type-K, 20-gauge thermocouple wires with ceramic fiber braid insulation, similar to those used on the surface of the slab. These

thermocouples were firmly fixed with high temperature resistant tape and aluminum foil tape to prolong the effectiveness of thermocouple temperature measurement during the vehicle fire. Some of the thermocouples were placed against surfaces to collect surface temperatures, while others were placed with the sensors hanging free to collect gas temperatures. Figure 4.4 shows the placement of thermocouples around the vehicle.

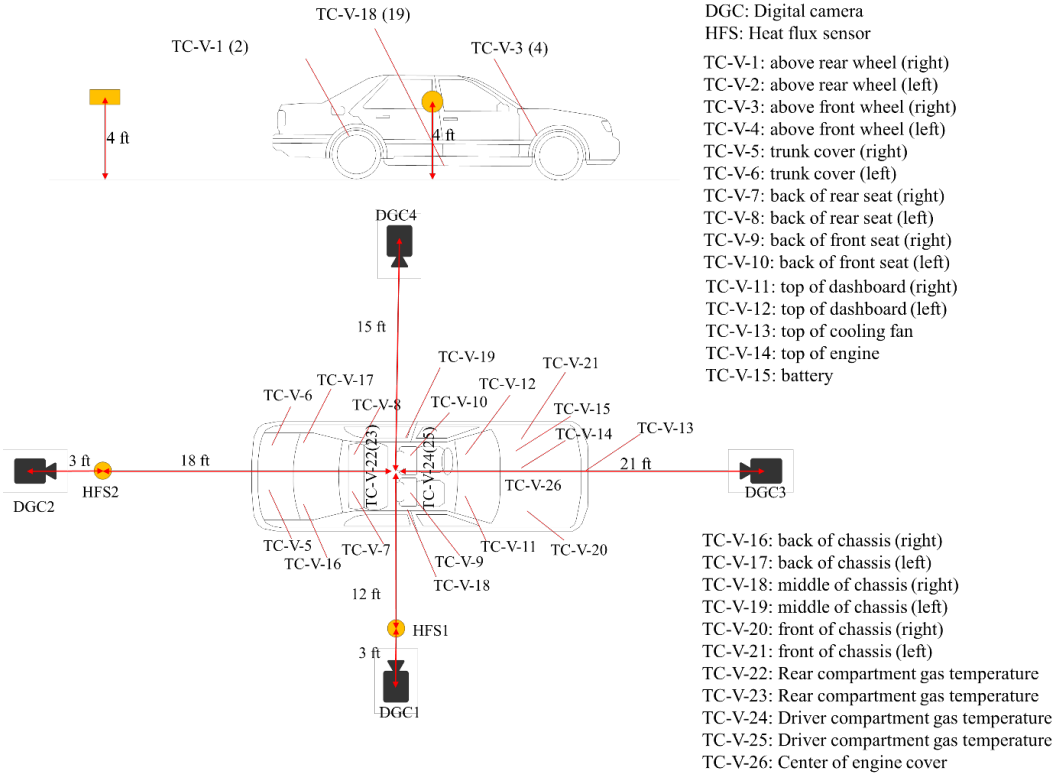

Figure 4.4 Locations of thermocouples placed in and around the test vehicle

Beyond temperatures, flame radiation is another important parameter to quantify the thermal harm of flame to the surrounding environment. Two heat flux meters were installed to measure the radiant heat flow at the back and on one side of the burning vehicle to quantify the heat radiation flux at these locations. These sensors were placed 12 feet from the center of the vehicle (around 9 ft from the edge) and 18 feet from the center (around 10 ft from the edge), at the side and rear, respectively, with both at a height of 4 feet from the panel surface, as shown in Figure 4.4. MedTherm 64 series water-cooled protection wide-angle heat flux sensors, with a range of 10kW/m^2, were used in the test [74]. These Schmidt Boelter type sensors measure both radiant heat flow and convective heat flow. During the experiment, the heat flow meters were continuously water cooled to ensure the accuracy of measurements. Cooling the heat flux gauges with water helped to ensure that their surfaces remain close to the ambient temperatures, maximizing the convective heat transfer and minimizing radiative losses. The gauges' surfaces are also coated with high emissivity paint to maximize the absorbed radiation. Figure 4.5 shows an example of a heat flux sensor used, and Table 4.2 gives the parameters of the sensor.

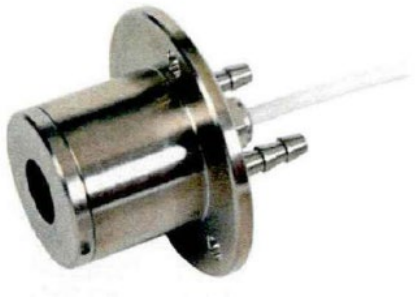

Figure 4.5 MedTherm 64 series heat flow meter

Table 4.2 Parameters of heat flux meter

Main parameter	Value
Diameter of heat flow meter	25 mm (0.98 in)
Temperature range of cooling water	10℃–30℃
Diameter of sensing zone	10 mm (0.39 in)
Scope of perspective	180°
Emissivity	>0.95
Sensor principle	Gardon and Schmidt-Boelter
Correction uncertainty	<±6.5% (confidence interval 95%, 5kW/m^2-100kW/m^2)
Response time	Measuring range 10kW/m^2: <200ms (63%)

In addition to measuring temperatures, it was also important to capture the visual aspects of the vehicle fire test. To do this, four video cameras were placed in strategic positions to capture different angles of the vehicle during the fire. The video cameras were placed on tripods and positioned to capture different angles of the vehicle during the fire, including the front, side, and rear views.

5. TESTS ON THE CONSTRUCTED BRIDGE DECK WITH OVERLAY

Several material and performance tests were planned to evaluate the change in characteristics and performance of the composite slab after exposure to a vehicle fire. These tests include skid resistance, surface hardness, delamination, bond strength, water penetration and abrasion resistance tests. The skid resistance test evaluated the changes in the coefficient of friction of the slab surface before and after the fire. Surface hardness tests evaluated the change in the surface hardness due to the fire. The delamination test gave an indication of the continued adhesion between the polymer concrete (PC) overlay and substrate concrete after exposure to the vehicle fire. The bond strength test offered an insight into changes in the strength of the bond between the PC overlay and substrate concrete due to elevated temperatures, while water penetration and abrasion resistance tests evaluated the ability of the slab to resist water penetration and abrasion, respectively, after the fire. Some of these tests, which are non-destructive in nature (specifically skid resistance, surface hardness, and delamination), were designated to be carried out at specific locations on the surface before and after the vehicle fire. The other tests, which would be destructive to the constructed slab, were planned to be carried out only after the vehicle fire, with the results compared to test cores collected before the fire.

Figure 5.1 shows the instruments and equipment used for the different tests. To determine control values for the destructive test, 4-inch cores were collected from an extension made to the main slab, constructed to the same specifications and at the same time as the area to be tested. Other cores were also made in this area to test the strength of the PC overlay to substrate concrete bond before the vehicle fire. These control tests enabled a comparison of the test results before and after the fire and quantitatively determined the changes to the PC material due to exposure to high temperatures. The locations for the pre-fire tests and the drilled cores are as shown in Figure 5.2, and the number of tests for each experiment is shown in Table 5.1.

(a)

(b)

(c)

(d)

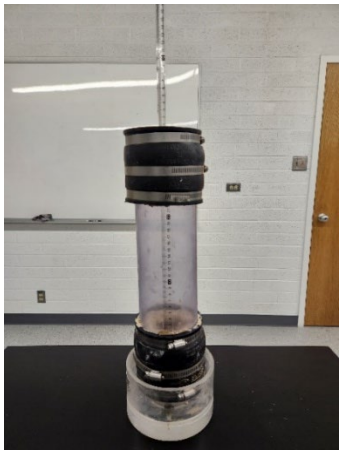

(e)

(f)

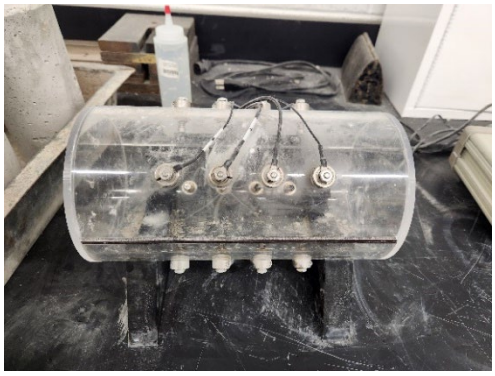

(g)

Figure 5.1 Instruments and equipment used for the performance tests: a) British pendulum tester for skid resistance, b) Rebound hammer for surface hardness, c) FLIR T640 IR camera for delamination, d) Proceq Dyna Z16, e) Falling head setup for water penetration, f) Setup for abrasion resistance tests, g) Wenner probe array for resistance to chloride penetration tests

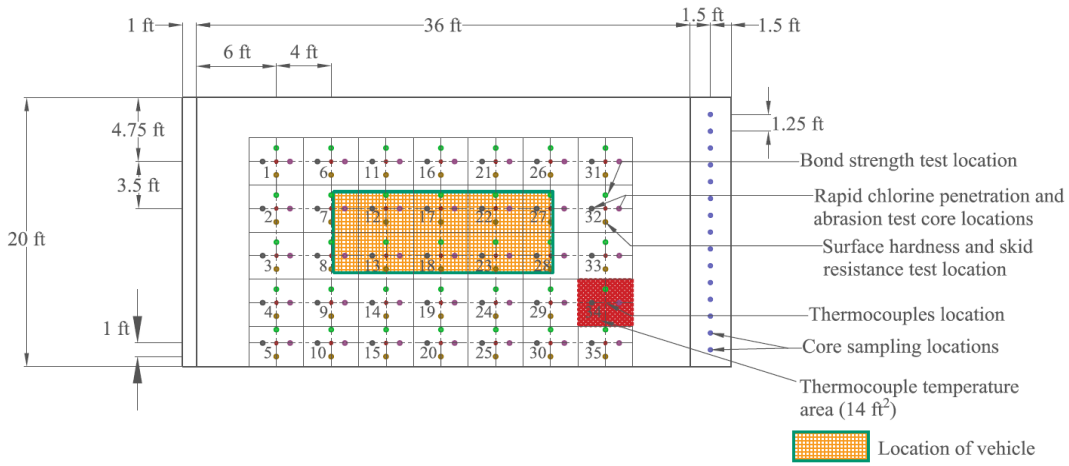

Figure 5.2 Test sampling locations (units in ft)

Table 5.1 Number and sizes of specimens for each experiment

Test	Specimen size	No. of control tests	No. of post-fire tests	ASTM Standards
Skid resistance test	N/A	35	35	ASTM E303 [66]
Surface hardness test	N/A	35	35	ASTM C805/C805 M [67]
Delamination test	N/A	N/A	N/A	ASTM D4788 [68]
Bond strength test	Disc size 2 in.	5	20	ASTM C1583/C1583M [69]
Water-penetration test	4 in. dia. with 4 in. height	6	6	ASTM D5084 [70]
Abrasion resistance test	4 in. dia. with 4 in. height	3	20	ASTM C944/C944M [71]
Rapid chloride penetration test	4 in. dia. with 4 in. height	6	6	AASHTO T 358 [72]

Core samples collected from the panel were prepared in accordance with ASTM C42 [75] by carefully wiping them after collection, sealing them in plastic bags, and placing them in a curing chamber for storage prior to testing. The specimens were tested at least five days after collection to ensure that any moisture gradients introduced while wetting the area during coring was removed. The test process used for each of the aforementioned tests are outlined below.

5.1 Skid Resistance

Carried out to determine the surface frictional properties of a pavement surface, this test essentially characterizes the ability of a surface to prevent a tire from sliding while driving on it. Executed in accordance with the ASTM E303 standard [66], the skid resistance is measured using a British pendulum tester shown in Figure 5.1a. For the test, the tester, consisting of a pendulum arm and a base assembly, is placed on the surface. The pendulum arm is then released from an elevated horizontal position and allowed to swing downwards and sweep the road surface and then continue upwards. A needle arm is connected to the pendulum arm and swings with it. On the upward swing, the needle arm is released from the pendulum arm at its peak before it returns. This needle arm points to the position of the highest

position the pendulum reaches on its swing. This position is registered as the British pendulum number (BPN) of the surface being test, with a high BPN indicative of a high skid resistance of the surface. The BPN resulting from this test is used as a representation of the skid resistance of a surface. This value is computed for a pavement as the average of tests carried out on several areas, as shown in Eq. 2.

$$\mathrm{BPN} = \frac{1}{\mathrm{n}}\sum_{\mathrm{i=1}}^{\mathrm{n}} \mathrm{BPN_i} \qquad \text{Eq. 2}$$

Where: *BPN* is the mean BPN, and *n* is the number of BPN tests at a location.

For a surface, a BPN value of 45 and above is required in order to be considered acceptable for vehicular traffic. This test was carried out at 35 locations, as shown in Figure 5.2, over the panel in order to obtain the skid resistances at these different locations, which were expected to be exposed to the elevated temperatures from the fire.

5.2 Surface Hardness

The hardness test is used to monitor the surface hardness of the pavement in order to determine its usability prior to opening it for traffic. Carried out in accordance with ASTM C805/C805M [67], this test requires that the surface meets a minimum Schmidt rebound number of 25 for the road surface to be passed as fit for service. The test involves the use of a rebound hammer, shown in Figure 5.1b, which is a steel cylinder wrapped around a mass and spring assembly. A plunger connected to the mass extends out of the casing. When the plunger is depressed, the mass is pushed into the hammer, extending the spring, until it hits a release mechanism. This releases the mass, which then drops back onto the plunger and rebounds upwards. The distance the mass rebounds is dependent on the hardness of the surface and is referred to as the rebound number. While testing, the hammer is held vertically over the surface to ensure that the plunger makes complete contact with the surface under investigation. The maximum hardness value for tests carried out in a single location is taken as the rebound number for that location, and the average of the rebound numbers at the different locations is taken as the rebound number for the entire pavement. Similar to the skid resistance test, this non-destructive test is carried out at 35 locations over the surface of the slab prior to and after the vehicle fire.

5.3 Delamination

Thermal imaging is a technique used to detect delamination in highway surfaces as per ASTM D4788 [68]. An infrared (IR) camera (as shown in Figure 5.1c) is used to collect thermal images of the surface, and any temperature differences greater than 0.5^{o}C between local regions are considered indicative of delamination. In this test, thermal images are collected over 4 ft x 4 ft areas of the surface, and the images are then stitched together to form a thermal map of the entire surface. Areas with delamination should appear as hot spots in the thermal images, and a comparison of the thermal images from before and after the fire test can reveal any areas where delamination occurred due to exposure to elevated temperatures. This test is non-destructive and can provide valuable insight into the structural integrity of the pavement overlay. To determine the efficacy of using an IR camera to capture delamination in overlays, small test specimens were designed and tested prior to the actual vehicle fire tests. The process used for these tests is detailed in the Appendix A.2.

5.4 Bond Strength

Used principally to determine the strength of the bond between an overlay and the substrate concrete, this test involves the application of a tensile force to an area of the overlay in a bid to pull it off the underlying concrete. Carried out in accordance with ASTM C1583/C1583M [69], direct pull off tests are conducted by first cutting through the overlay and concrete with a core drill. Next, a steel disc is attached to the surface of the cut section and the adhesive is allowed to cure. Once proper adhesion is achieved, the tensile loading device shown in Figure 5.1d is attached to the disc and the tensile force applied at a constant rate until failure. Both the failure load and failure mode are recorded, and the bond strength is determined as shown in Eq. 3.

$$\text{Bond or Tensile Strength} = \frac{\text{Tensile load}}{\text{Area of test specimen}} \quad \text{Eq. 3}$$

With its destructive nature, this test could not be carried out on the area where the vehicle fire test was to take place prior to the fire test. To this end, five tests were carried out on the added area of the slab under the assumption that this area would have very similar characteristics to the rest of the slab, as they were constructed together. Post fire, the locations deemed to have had the highest exposure to the vehicle fire were tested to determine the change in bond strength and characteristic bond failure type.

5.5 Water Permeability

The water permeability test is used to determine the ability of the PC overlay to resist water ingress and is conducted according to the ASTM D5084 [70]. The test entails measuring the rate at which water permeates through a specimen. To perform the test, a sample is placed in a vacuum pump and water is pumped through until it is fully saturated. The sample is then sealed into a no-hub connector and a graduated cylinder is attached to the opposite end. Water is poured into the cylinder, and the initial and final water levels are recorded after a period. The change in water level is used to determine the relative permeability coefficient of the sample using Darcy's law, as shown in Eqs. 4 and 5 [76].

$$dQ = dh\, a/h_1 t = kA\, h/L \quad \text{Eq. 4}$$

$$k = aL/At \int_{h_0}^{h_1} 1/h\, dh = \frac{aL}{At} \ln(h_1/h_0) \quad \text{Eq. 5}$$

Where: k is the coefficient of permeability, a is the cross-sectional area of the small tube, A is the cross-sectional area of the specimen's surface, h_0 and h_1 are the initial height of water and final height of water, respectively, L is the height of the sample, and t is the duration of the test.

Concrete specimens can have large variations in water permeability due to the nature of the materials it is composed of. This can make it difficult to properly characterize the change in water permeability after exposure to a vehicle fire, as the values would vary across different specimens. To reduce the uncertainties in the water permeability resistance due to sample composition, the relative permeability value using the falling head permeameter principle is measured for the same samples before and after exposure to heat, so that any computed change in permeability can be attributed to the exposure to heat and not to changes in the composition of the specimen.

5.6 Abrasion Resistance

The abrasion resistance test is a method used to evaluate the durability and longevity of a surface by measuring its resistance to wear and tear caused by friction and impact. This test is performed in accordance with the ASTM C944/C944M [71]. The test apparatus consists of a rotating cutter, which is attached to a drill press, as shown in Figure 5.1f. The cutter is composed of a series of dressing wheels that are mounted on a rod, which is connected to the drill press. The cutter is rotated at a speed of 200 revolutions per minute (RPM) during the test.

A test specimen, which is a representative sample of the surface to be evaluated, is first weighed and placed under the drill bit. The cutter is then placed on the surface of the specimen and run over it at a minimum speed of 200 RPM for two minutes while exerting a force of 98 N. This allows the dressing wheels to wear down the surface of the specimen. After the test, the change in weight of the specimen is determined and taken as the measure of its resistance to abrasion.

5.7 Rapid Chloride Penetration

Conducted in accordance with the AASHTO T358 standard [72], this test aims to determine the resistance of concrete to chloride ingress. Permeation of chlorine through concrete surfaces could lead to corrosion of reinforcing steel, leading to reduction in the strength of reinforced concrete members. Thus, this quality control test is carried out to ensure that the panel is impermeable to chloride ingress. The test is carried out using a Wenner probe array (Figure 5.1g) to determine a resistivity value for a sample. Samples to be tested are placed in a water bath for 24 hours to ensure a saturated test surface. The Wenner probe array is then placed along the length of a sample, and a reading of electrical resistivity taken. This is repeated three times, turning the sample 90^{o} for each set of readings. The electrical resistivity is computed as the average of these four values. The chloride ion penetration can then be classified from the resistivity using Table 1 in AASHTO T 358 [72].

The Wenner probe array is specifically engineered for assessing the resistivity of specimens along their length. Consequently, it is not suitable for testing core specimens extracted from the concrete slab. To address this limitation, custom specimens exclusively for RCPT evaluations were cast. These specialized specimens consisted of 3-inch diameter concrete cylinders encased in PC with an average thickness of 0.5 inches. This design enabled a replication of the PC overlay conditions on a concrete substrate within a cylindrical sample. These specimens were tested by heating them in a furnace to temperatures replicating some of those recorded in the vehicle fire test.

6. VEHICLE FIRE TEST RESULTS AND DISCUSSION

6.1 Burning Process

Before the vehicle fire test, 2.4 gallons of gasoline were poured into the gas tank. The plug over the drilled hole was removed to allow the gasoline to leak onto the panel surface. The pooled leaking gasoline was then ignited using a flare and the vehicle was allowed to burn for 225 seconds before the test was stopped. The progression of the fire was recorded and described in Table 6.1 and shown in Figure 6.1. The ignition of leaked gasoline sparked a rapid propagation of fire on the panel, subsequently engulfing the vehicle and spreading throughout its interior and exterior. As the gasoline vaporized into combustible gas and filled the gas tank along with oxygen, it was ignited by an external flame. This caused a jet of flame to erupt from the gas tank. The fire was put out following the jet flame. In addition to the heat from the burning vehicle to the panel, certain portions of the panel were exposed to direct contact with flames due to the presence of leaked gasoline, which burned on the panel surface. Additionally, the melting plastic material from the vehicle also contributed to the direct burning on the panel surface.

Table 6.1 Process of the vehicle fire

Time (s)	Events	Time (s)	Events
0	Ignition of gasoline on the panel close to rear of vehicle and flames spread on the panel over the area with gasoline.	162	Flames surge through the crevices between the front windshield and the vehicle's body, as well as seep through the fractures in the windshield itself.
52	Flames begin to spread into the interior of the vehicle	167	Flame fully engulfs the exterior of the vehicle except the hood, and more sections of the panel were directly exposed to flames due to the continuous falling of melted plastic from the vehicle.
57	More sections of the panel were directly exposed to flames as melted plastic falls from vehicle onto panel and burns on the panel surface directly.	213	Jet flame from the gas tank.
72~79	Brittle fracture of rear left window occurs, leading to flames inside the vehicle spreading outside and engulfing the top of the vehicle exterior.	220	Small explosions due to ignition of the front airbags.
138	Small explosions due to the ignition of rear airbags.	225	Firefighters began to put out the fire

Gasoline allowed to leak

0 seconds (ignition)

52 seconds

57 seconds

72~79seconds

138 seconds

162 seconds

167 seconds

213 seconds

220 seconds 225 seconds

Figure 6.1 Burning process of the vehicle fire

Figure 6.2 shows the burned vehicle after the test. Most of the vehicle sustained significant damage, but the front and engine compartment were relatively undamaged due to the intervention of firefighters to put out the fire. Later examination of temperature data shows that the temperatures within the engine compartment did not rise significantly. The short duration of the fire limits the possibility of extrapolating the results to longer lasting fires and the response of PC overlays exposed to such scenarios. Also, during the test, firefighters consistently used water hoses on surrounding infrastructure to keep them cool and prevent the spread of the fire beyond the panel. The water from the hoses could potentially have affected the vehicle fire.

Figure 6.2 Burned vehicle

6.2 Vehicle Fire Exposure

A vehicle fire on a bridge or roadway can have an effect on its surrounding civil infrastructure such as girders, cables, and piers. Figure 6.3 shows the incidental heat fluxes measured at two specific locations, 12 feet from the center of the vehicle and 18 feet from the center, with both at a height of 4 feet from the panel surface.

The plot for the sensor at the side of the vehicle shows some distinct peaks. The first distinct peak at 92 seconds came just when the flames had begun to engulf the exterior, leading to the exposure of surrounding infrastructure to heat generated by the fire. A maximum heat flux of 16.9kW/m^2 was recorded at this time. At 225 seconds, another distinct peak occurs, reaching 47.5 kW/m^2. This increase

corresponds to the period of intense burning when the vehicle fire intensified due to the jet flame emanating from the gas tank.

Similarly, the plot for the sensor at the rear of the vehicle shows a distinct peak of 18.1kW/m^2 at 199 seconds. This peak occurred shortly after flames fully engulfed the exterior leading to heightened heat transfer to surrounding areas. A second distinct peak of 26.7 kW/m^2 at 224 seconds occurred just after the jet flame from the gas tank ignition. The maximum heat flux recorded by the heat flux sensor placed at the back of the vehicle was just over half of that recorded by the sensor at the side. This can be attributed to multiple factors, including the shorter distance between the side heat flux sensor and the vehicle's edge, the sensor's proximity to the fuel tank, and the potential influence of wind direction. Overall, these peak incidental heat flux measurements fall in line with what has been observed in other vehicle fire tests [58, 77, 78], and offer a glimpse into the potential adverse effect of vehicle fires on surrounding infrastructure.

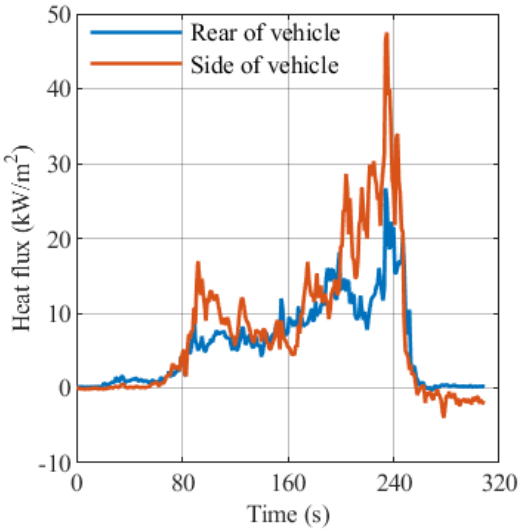

Figure 6.3 Heat flux from vehicle during test with maximum heat fluxes recorded at 224 s and 225 s at the back and side of the vehicle, respectively

Figure 6.4 shows the temperature history of different locations inside the vehicle. Two distinct patterns can be seen in the temperature evolution over the test period. First, the area of the vehicle, between the dashboard and the trunk, shows a steady increase in temperatures as the fire spread and burned through the interior of the vehicle. These areas were significantly damaged as the fire progressed toward the front of the vehicle. On the other hand, the regions surrounding the vehicle engine showed minimal temperature increases, as these areas were farthest from the point of ignition and were not ignited before the fire was extinguished. The highest temperatures recorded were gas temperatures in the interior of the vehicle, which peaked at around 1,200°C, while the lowest peak temperature was just over 40°C at the top of the battery in the engine compartment. Moreover, at some locations such as the chassis that was close to the panel, the temperatures peaked and evened out at about 160 seconds into the test and remained relatively steady until the fire was put out; while at other locations such as the interior spaces, temperatures continued to rise, peaking out when the jet flame from the gas tank occurred.

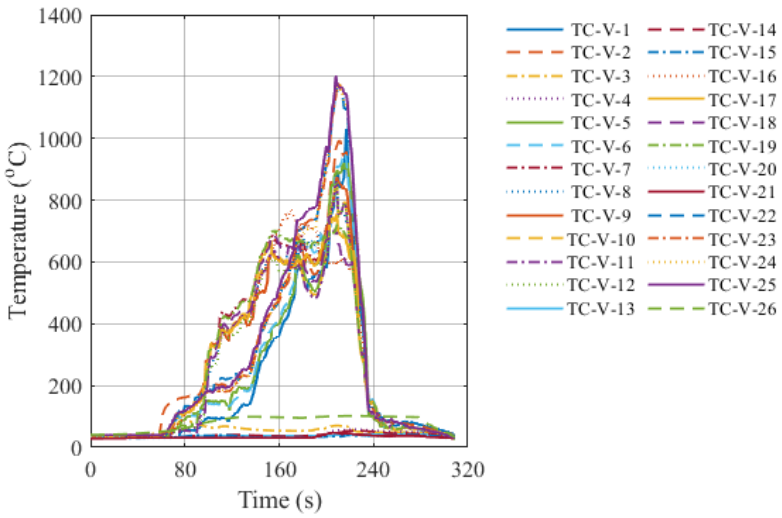

Figure 6.4 Temperature evolution at different locations inside the vehicle

6.3 Heat Exposure of Polymer Concrete Slab

After the vehicle fire, the burnt vehicle was removed from the panel and the surface cleaned of debris using water and a brush. Figure 6.5 illustrates the extent of damage caused by the vehicle fire on the panel after the surface was cleaned. It is evident that the fire damage is concentrated in the area directly under and around the vehicle's location. This is due to the proximity of this area to the burning vehicle. It was observed that some of the finishing sand placed on the PC overlay had started peeling off due to the degradation of the polymer resin and the water flushing. The polymer resin in some parts of the panel surface experienced thermal decomposition, leaving the surface charred. Other parts of the panel surface do not show these effects. The subsequent observation of the temperatures recorded in different areas reveal that the areas showing these visible effects were also those which recorded significant temperature increases. As a result, the post-fire investigation of the panel's properties was focused on this specific area.

Figure 6.5 Post-fire surface of the panel

The vehicle fire caused temperatures to rise at different locations on the panel as the fire spread. Measured by thermocouples placed at the locations delineated in Figure 3.6, each thermocouple was placed 3.5 ft by 4 ft apart, and thus the temperatures measured by each are assumed to be the average temperature over an area of 14 ft^2. Figures 6.6 and 6.7 provide a detailed view of how these temperatures changed over time and the spatial distribution of the maximum temperatures, respectively. From Figure 6.6, there are two distinct patterns in the temperatures recorded. Areas close to the vehicle recorded extremely high temperatures, with a maximum of 744ºC recorded. On the other hand, areas farther away

from the vehicle recorded much lower temperatures. Generally, areas within a few feet of the vehicle in all directions recorded significant temperature rise, indicating exposure to high levels of heat from the fire. For areas that experienced significant temperature rise, two peaks in temperature were recorded. The first peak, predominantly observed within the initial 100 seconds, is linked to the ignition of the leaked gasoline and the burning of falling plastic on the panel. This initial combustion ceased when the fuel load on the panel was exhausted, indicated by a marked decrease in temperature. However, temperatures soon began to escalate once more as the fire proliferated throughout the vehicle and more melting plastic dropped onto the panel. This exposed additional surface areas to more severe fire exposure (including direct flame contact), resulting in heightened temperatures. The second peaks observed between 189 seconds and 247 seconds for different thermocouples can be attributed to the fire engulfing the vehicle, causing more plastic debris to fall onto the panel and burn directly on the surface. This is also accompanied by a jet flame from the gas tank around 213 seconds. Even after the onset of firefighting efforts, certain peaks were observed because the process of extinguishing a fire is not instantaneous. Figure 6.7 provides a visual representation of the distribution of the maximum temperatures at the surface. Significant temperature increases were recorded in a small area around the location of the vehicle.

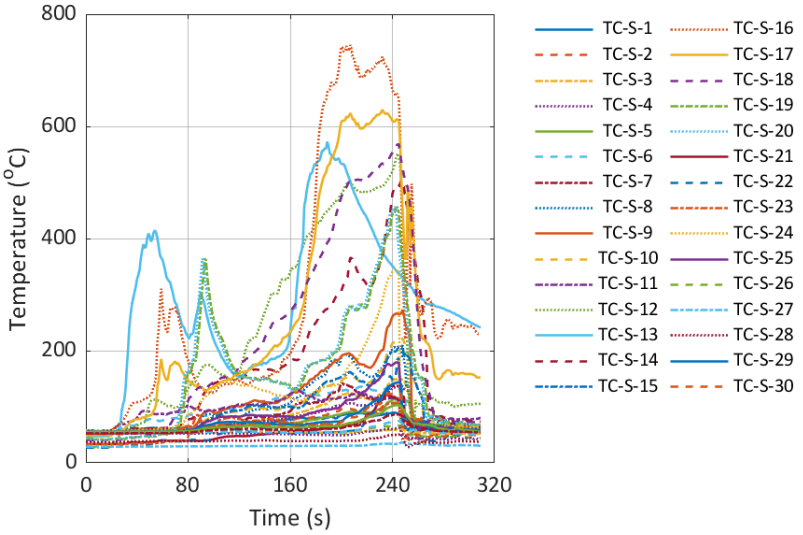

Figure 6.6 Temperature evolution at surface of overlay over time of the vehicle fire test

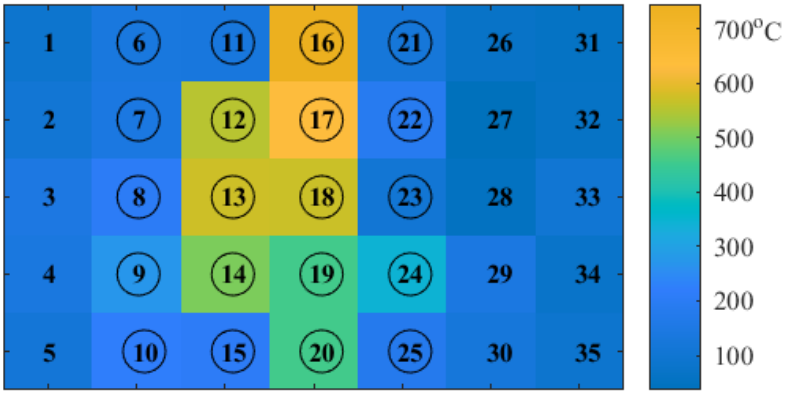

Figure 6.7 Maximum recorded temperature at different locations over the surface (circles shows the locations for post-fire test sampling)

According to the surface damage of the panel (shown in Figure 6.5) and the recorded maximum temperatures at the panel surface (shown in Figure 6.7), these areas with severe heat exposure were identified. Further investigations into the post-fire performance of the PC overlay were focused on these areas and their surroundings, highlighted by circles in Figure 6.7. Core samples were collected from the designated areas (shown in Figure 5.2) to evaluate the impact of vehicle fire exposure on abrasion resistance and rapid chloride penetration of PC overlay. For non-destructive tests (skid resistance, surface hardness and delamination), the same areas where pre-fire tests were carried out over the slab were used, regardless of the level of exposure to the fire.

Figure 6.8 shows the temperature evolution at the interface between the PC overlay and substrate concrete, while Figure 6.9 shows the maximum temperature recorded at the interface across different locations. The interface temperature barely rises despite the exposure of the surface to elevated temperatures. It began to rise just as the test ended, indicating that the heat was starting to transfer through the overlay and onto the substrate concrete. These results suggest that PC overlays offer some thermal protection to structural concrete in highways and bridge decks at high temperatures by slowing down the transfer of damaging heat to the concrete.

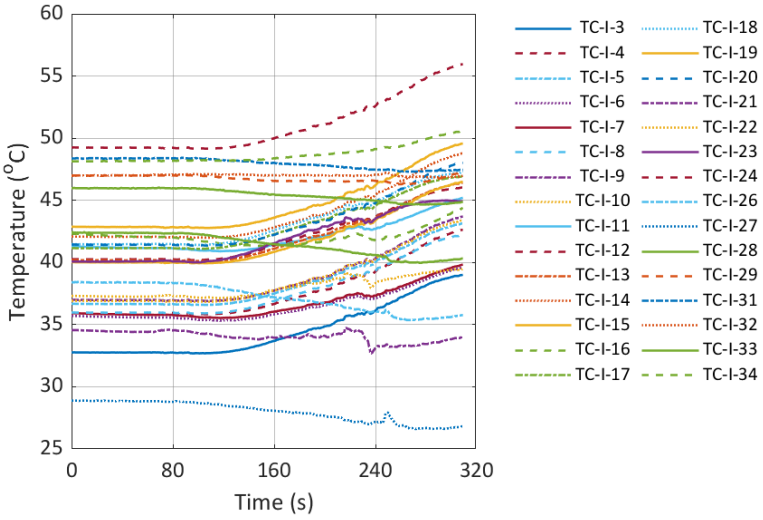

Figure 6.8 Temperature evolution at interface between overlay and concrete during the vehicle fire test

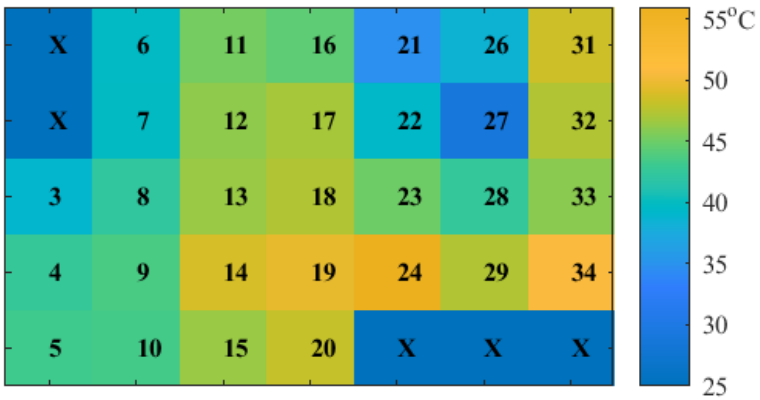

Figure 6.9 Maximum recorded embedded temperature distribution (X's indicating locations where no thermocouple was installed)

7. POLYMER CONCRETE PERFORMANCE RESULTS

7.1 Skid Resistance

The non-destructive nature of the skid resistance test allowed it to be repeated in the same locations before and after the vehicle fire. Skid resistance of a surface is determined as the average of measurements taken at different locations over a surface. Figure 7.1 presents the BPN at each test location before and after the fire. The colors on the figure represent the maximum temperatures recorded at each location during the fire. The numbers in each location are the location index, the pre-fire BPN (in green), and the post-fire BPN (in red and brackets). The results presented in Figure 7.1 demonstrate the negative impact of fire on the skid resistance of the PC overlay. Prior to the vehicle fire test, the average skid resistance recorded as BPN at all 35 locations over the surface was 59.89. This value dropped to 48.32 after the vehicle fire test, representing a 19% reduction in the skid resistance. Comparatively, for areas registering high maximum surface temperatures (represented by the areas selected for post-fire testing and circled in Figure 6.7), the skid resistance dropped from a pre-fire average of 59.25 to a post-fire value of 45.3, representing a 24% decrease. Although the average BPN over the surface still exceeds the nominally acceptable value of 45, the notable drop from its pre-fire value is indicative of the negative effect of the fire on the skid resistance of the PC overlay.

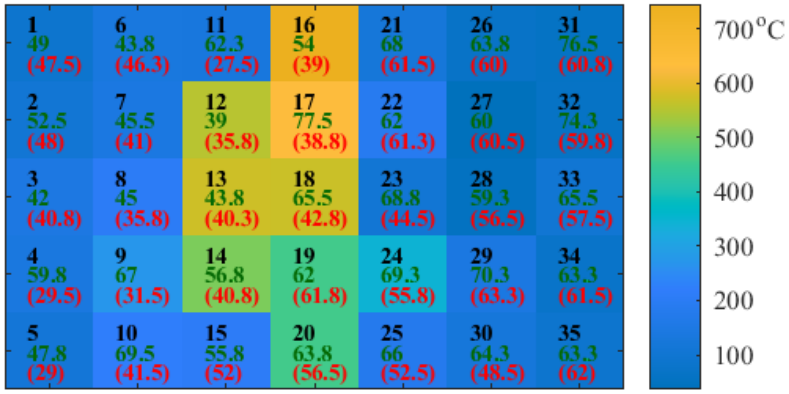

Figure 7.1 Pre-fire and post-fire skid resistance results (green values are pre-fire skid resistance and red values are post-fire skid resistance)

7.2 Surface Hardness

Similar to the skid resistance test, the surface hardness tests were carried out on the same locations prior to and after the vehicle fire test. Figure 7.2 presents the results of these non-destructive tests at the specific locations where they were conducted both before and after the vehicle fire. The figure includes a thermal map of the surface with the maximum recorded temperature at each location, the location indices, and results (pre-fire results are in green and post-fire results are in red and brackets) for the surface hardness tests. A decline in the surface hardness due to the fire exposure can be observed across the surface. Over the entire surface, this resulted in an average drop in hardness from 48.8 to 45.7, representing an 8% decrease. Within the areas exposed to very high temperatures from the vehicle fire (between locations #6 and #25, as indicated in Figure 6.7), this change was more pronounced with the surface hardness reducing from 48.8 to 43.6 after the vehicle fire, representing an 11% drop in surface hardness.

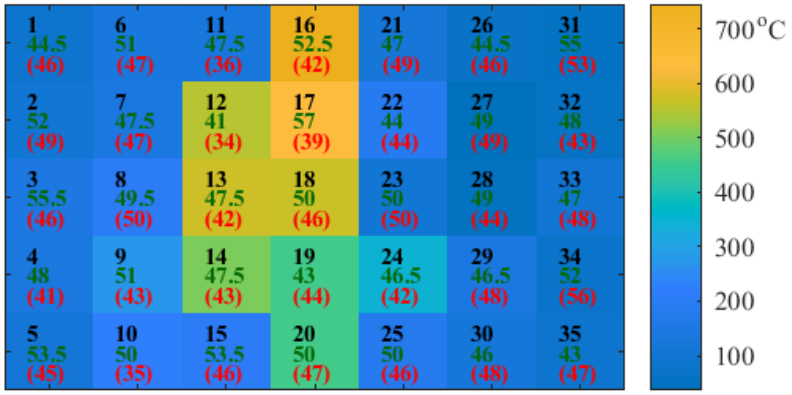

Figure 7.2 Pre-fire and post-fire surface hardness results (green values are pre-fire surface hardness and red values are post-fire surface hardness)

7.3 Delamination

The significant discrepancy in thermal expansion coefficients between concrete and PC may induce delamination at elevated temperatures. This could potentially compromise the bond between the PC overlay and its underlying concrete substrate. An FLIR T640 thermal imaging camera was used to capture the temperature distribution over the surface, and this information was used to evaluate the presence of delamination. Areas exhibiting substantially higher temperatures (exceeding half a degree compared with the surrounding) are identified as hot spots, indicating delamination. These tests were performed over small areas of the panel at a time (4 ft x 4 ft). It is important to note that before the tests, the surface was exposed to sunlight and daytime temperatures for at least three hours, as per ASTM D4788 [68].

Figure 7.3a and 7.3b depict the thermal maps of the surface before and after exposure to the vehicle fire, respectively. To enhance contrast, a Gaussian filter was applied to the original images. The process of capturing thermal images across the entire surface took over an hour on average, during which changes in environmental conditions could occur and influence surface temperatures. This phenomenon is particularly evident in Figure 7.3a, where distinct temperature variations are observed across different regions of the panel. In addition, although efforts were made to ensure that post-fire measurements were conducted under similar environmental conditions to those before the fire (starting to collect the images after midday when the sunlight had passed overhead and the entire surface had been exposed to more than three hours of sunlight), it was inevitable to encounter some degree of variability in the environmental conditions at both times.

To minimize the impact of such variations and facilitate the identification of hot spots indicative of delamination, the average temperature recorded in one sub thermal image was subtracted from all the temperature values captured in that image before stitching all sub images together to form the thermal map of the entire panel surface. The resulting pre-fire and post-fire thermal maps are shown in Figures 7.3c and 7.3d, respectively. Despite improvements, detecting delaminated areas remains challenging due to the presence of significantly low-temperature regions. This causes all other areas to appear relatively hot, making it difficult to identify the true hot spots. To address this, maps were created to isolate regions that are at least 0.5°C hotter than the surroundings (the average temperature of each sub image). Those regions are highlighted in yellow in Figures 7.3e and 7.3f. Prior to the fire test (Figure 7.3e), some hot spots were observed around the panel, which can be attributed to construction related defects. However, after the vehicle fire (Figure 7.3f), a substantial increase in hot spots was evident, suggesting that the vehicle fire had likely caused delamination of the overlay from the underlying substrate concrete. While no additional tests were conducted to confirm the presence or otherwise of delamination, subsequent bond strength tests (shown in Section 7.4), and prevalence of debonding rather than concrete fracture, in these

areas further support the conclusion of delamination presence across the panel surface. Since the post-processing method is equivalent to identifying hot spots for each sub thermal image by comparing each pixel's temperature with the average temperature of that specific sub image, it may hide some large delamination that extends across an entire sub thermal image. To address this problem, Figure 7.3g and Figure 7.3h highlighted the hot spots when comparing the temperature of each hot region, 12, 13, 14, 16, 17, 18, 19, 20, and 24, (indicated in Figure 6.7) with the average temperature of the surrounding cool regions. It was noted that the regions exposed to high temperatures during the vehicle fire tests exhibited hot spots, which could potentially indicate delamination.

Although the described processing steps helped mitigate the effect of environmental variations, they did not entirely eliminate these effects. Ideally, alternative methods such as using UAVs to capture thermal images of the entire panel in a single thermal image could further mitigate this issue, reducing the impact of environmental changes, and ensuring that the temperature differentials obtained are more reliable for assessing delamination.

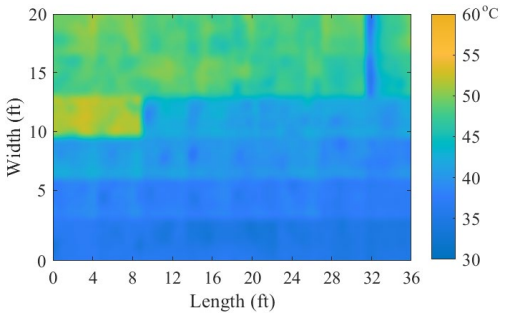

(a)

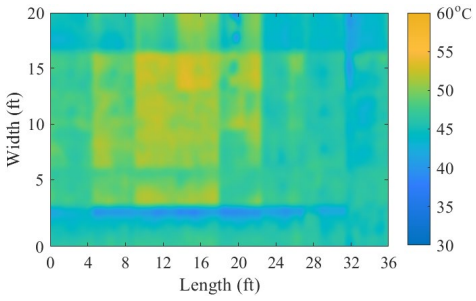

(b)

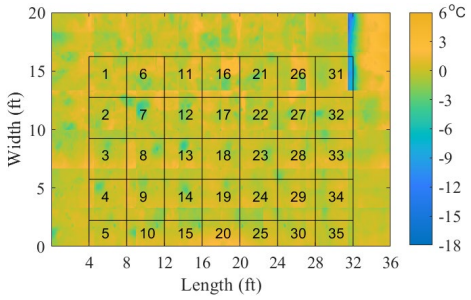

(c)

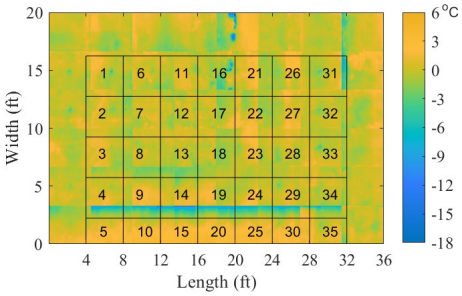

(d)

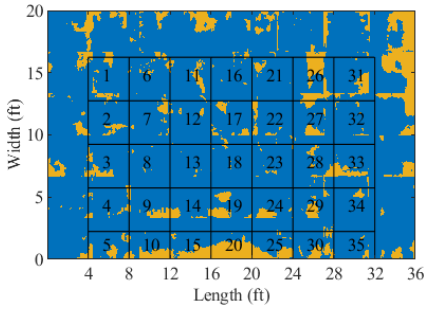

(e)

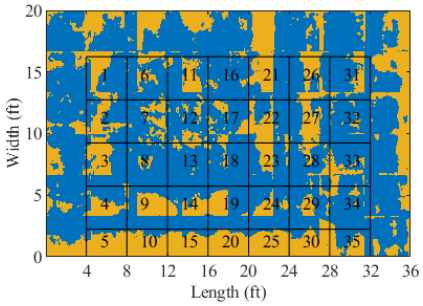

(f)

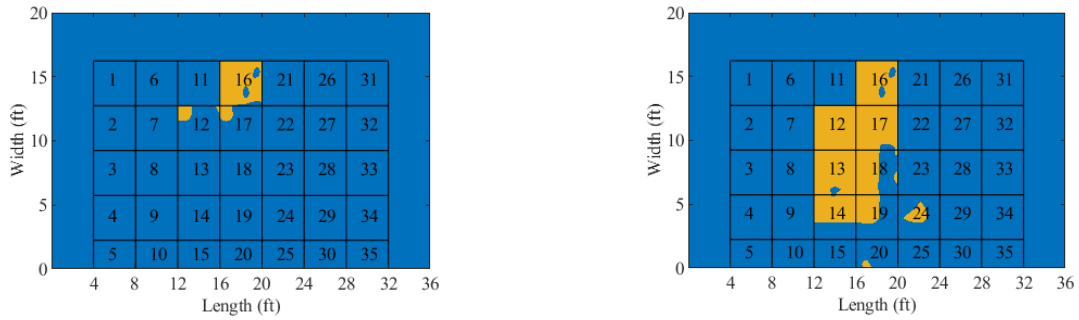

(g) (h)

Figure 7.3 Panel surface a) thermal map before fire exposure, b) thermal map after fire exposure, c) thermal map before fire test with average temperatures subtracted, d) thermal map after fire test with average temperature subtracted, e) hot spots before fire exposure identified within each sub image, f) hot spots after fire exposure identified within each sub image, (g) hot spots before fire exposure identified by comparing hot areas with cool areas, (h) hot spots after fire exposure identified by comparing hot areas with cool areas.

7.4 Bond Strength

To determine the nominal bond/tensile strength of the PC overlay to the concrete substrate, five tests were carried out at the added-on section of the slab. Failures that occur in the substrate concrete are recorded as tensile strengths, while those that occur in the bond between both materials are recorded as bond strength. The resulting strengths from these tests range from 298 psi to 327 psi. The resulting average strength of the samples was computed as 312.7 psi. Four of the tests resulted in failure in the substrate concrete and one resulted in failure in the bond between the overlay and the substrate concrete. This indicates that the bond strength of the overlay exceeds the tensile strength of the underlying concrete. Figure 7.4 provides examples of the two different failure modes as they occurred at different areas of the surface. After the vehicle fire, similar tests were carried out around the locations marked out in Figure 6.7, and the failure modes recorded for these tests are shown in Figure 7.5. In the figure, the colors represent the maximum temperatures recorded during the test, and the circled numbers indicate areas where the failure mode was bond failure. It is evident that bond failure prevailed in the tested regions of the panel, rather than concrete breakout, which differs from the findings of the pre-fire tests. The increased observed bond failures indicate a clear reduction in bond strength due to heat exposure. Notably, these areas experiencing bond failure align with the regions exposed to the highest temperatures during the vehicle fire test.

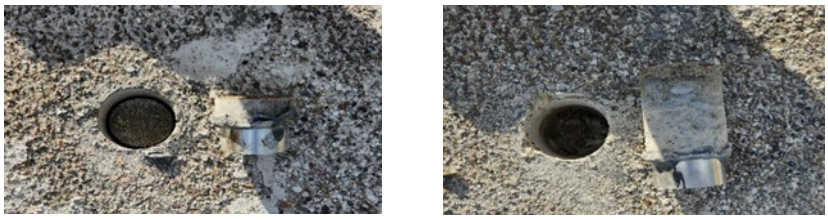

(a) (b)

Figure 7.4 Failure modes recorded during bond strength tests a) bond failure and b) failure in substrate

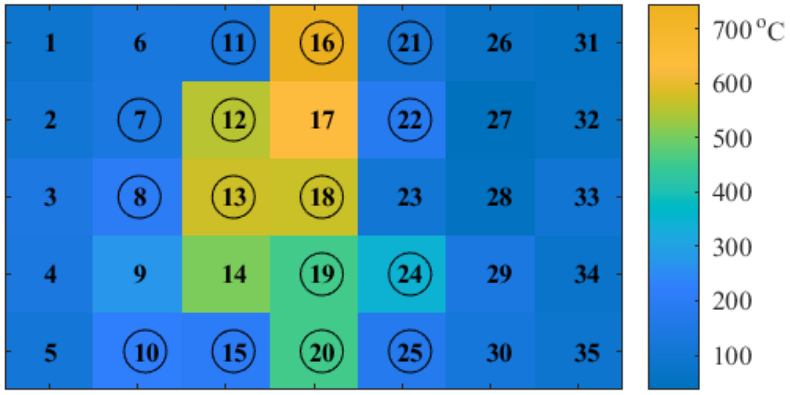

Figure 7.5 Failure mode in bond strength test (colors represent the maximum recorded temperatures, and the circles around numbers represent locations with bond failure).

7.5 Water Penetration

As explained in Section 5.5, the water penetration test was carried out on the same samples before and after heat exposure to eliminate any variability in coefficient of permeability attributable to variations in material composition among different samples. The coefficients of permeability in the water penetration tests were determined using the falling head principle. Each sample was insulated leaving only the PC surface exposed, as shown in Figure 7.6, and then exposed to one of two different temperatures (350ºC and 700ºC) for a specific duration (60 seconds, 180 seconds, and 300 seconds) at a rate of heating of 3ºC/s to mimic the exposure of the panel to high temperatures during the vehicle fire test.

The falling head test was repeated after allowing the samples to cool down to ambient temperature, and the relative change in permeability at different temperatures computed and used to characterize the change in permeability of the PC overlay after exposure to high temperatures. The results of water penetration tests are shown in Table 7.1. Table 7.1 shows a notable increase in the coefficients of permeability in the samples after the vehicle fire test. As the duration of heat exposure increases, so does the relative increase in permeability, with a particularly high 370% increase in this value for those samples exposed to 700ºC for five minutes. This indicates a reduction in the ability of the overlay to resist water ingress after exposure to high temperatures. This increase in permeability also increases the exposure of the substrate concrete to water and chemicals, which can lead to further damage and deterioration of the panel.

Figure 7.6 A core sample with PC overlay insulated before exposing to heat in a furnace

Table 7.1 Water penetration results

Temperature	Duration of exposure (s)	Coefficient of permeability (m/s)		Percentage change (%)
		Pre-fire	Post-fire	
350°C	60	9.98E-15	1.57E-14	57.06
	180	1.52E-14	2.57E-14	68.46
	300	7.97E-15	1.72E-14	115.30
700°C	60	1.32E-14	2.74E-14	107.95
	180	1.13E-14	4.41E-14	290.77
	300	1.14E-14	5.38E-14	370.78
Average		1.15E-14		

7.6 Abrasion Resistance

The abrasion resistance of a sample is determined by measuring the amount of material removed using rotating cutters. This is done by comparing the weight of the sample before and after running the cutters on its surface. For the pre-fire tests, five core samples were tested, and the average weight loss of the samples was computed. This average value is considered as the expected weight loss for the PC surface and describes its abrasion resistance. After the vehicle fire, a core sample was collected from each location marked in Figure 6.7 and tested. The results of the abrasion resistance tests, including both the pre-fire average value and the post-fire location-specific values, are presented in Figure 7.7. Each location on the figure includes a location index number, the average change in weight of core samples prior to the vehicle fires (in green), and the change in weight of the sample collected at the location after the vehicle fire (in red and brackets). The background color of each area represents the maximum temperature recorded in the area. The weight loss after abrasion testing was found to be greater in the samples that were exposed to the vehicle fire compared with the pre-fire average (4.5g weight loss for samples before the vehicle fire compared with 5g weight loss after the fire, representing an average of 11% increase in weight loss). This suggests a reduction in the abrasion resistance of the overlay. This decrease in abrasion resistance can be attributed to thermal degradation of the polymer matrix, resulting in a reduction of mechanical properties and increased susceptibility to wear and tear. This could lead to a reduction in the service life of the overlay and the need for regular maintenance and repair.

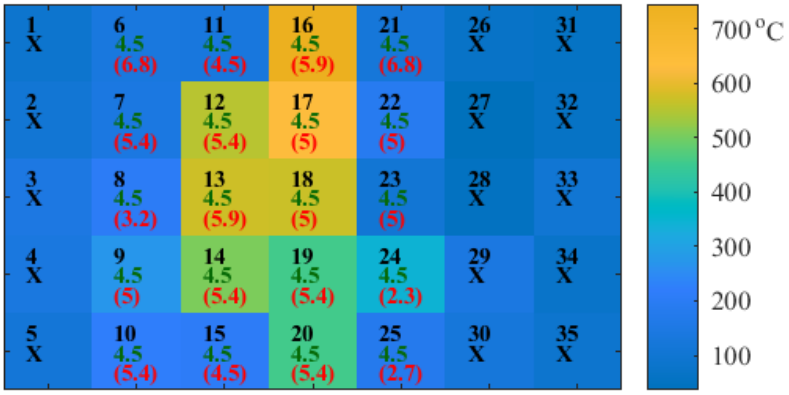

Figure 7.7 Pre-fire and post-fire abrasion resistance results. The change in weights overlaid on the surface temperature map (green values are pre-fire weight changes and red values are post-fire weight changes. "X" indicates areas where no cores were taken) (units are grams).

7.7 Rapid Chloride Penetration

Using the Wenner probe, the resistivities of six specimens were determined before and after exposure to elevated temperatures. After collecting the resistivities of the specimens, they were exposed to two different temperatures (300ºC and 500ºC) using heating rates replicative of the heating rates from the vehicle fire tests. Limitations of the equipment used meant that it was not possible to get the specimens heated to the maximum temperatures achieved in the actual vehicle fire tests. However, the use of similar heating rates and the attainment of high temperatures far exceeding the gas transition temperature of PC mean that the tests should adequately characterize the behavior of PC overlays on exposure to a vehicle fire. Figure 7.8 shows a sample in the test setup.

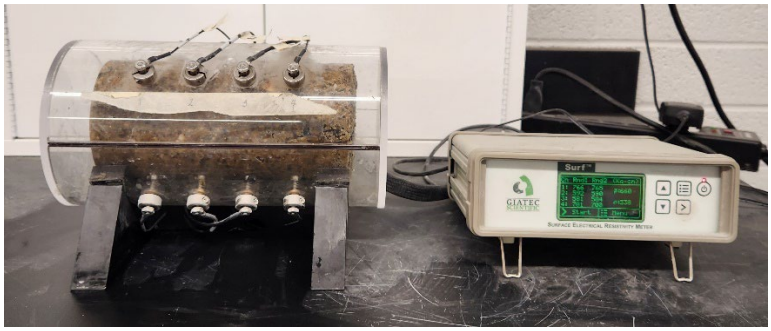

Figure 7.8 Sample in the Wenner probe setup to test for resistivity to chloride penetration

Table 7.2 shows the results from these tests. AASHTO T-358 specifies that surface resistivity above 254 kΩ-cm indicates that a material would have minimal chloride penetration. The results show that the average resistivity of the overlay before the fire was 745.1 kΩ-cm and thus the chloride penetration is rated minimal. After exposure, this resistivity dropped significantly by an average of 31.1% for samples exposed to 300ºC and 50.7% for samples exposed to 500ºC. These results indicate that heat exposure leads to a decline in the PC overlay's ability to withstand chloride penetration.

Table 7.2 RCPT test results before and after exposure to elevated temperatures

Temperature (ºC)		Resistivity (kΩ-cm)		Percentage change (%)
	Sample	Pre-fire	Post-fire	
300	1	671.25	490.38	26.95
	2	767.00	490.63	36.03
	3	719.13	501.33	30.29
500	1	749.00	378.75	49.43
	2	745.13	355.75	52.26
	3	750.06	372.11	50.39

7.8 Summary of Results

The results obtained from the performance tests carried out over the surface of the PC overlaid slabs exposed the susceptibility of PC to high temperatures. This vulnerability was evident across different properties with significant degradations observed after exposure. Table 7.3 summarizes the change in these different properties for tests conducted on specimens collected from the PC overlaid slab.

Table 7.3 Percentage change in properties after vehicle fire test

	Average change in property (%)			Maximum change in high temperature areas (location shown in brackets) (%)
Tests	Over entire panel	In high temperature areas and surroundings	In high temperature areas	
Skid resistance	19.3	23.6	23.1	34.7(18)
Surface hardness	7.5	10.7	13.3	31.6 (17)
Abrasion resistance	-	10.6	20.2	30.2 (16)

Table 7.3 reveals a clear trend of PC properties degrading after exposure to a vehicle fire, especially in areas experiencing high temperatures. This lends credence to a relationship between the exposure temperature and degree of degradation of PC properties. Similar patterns emerged in the tests carried out under controlled conditions. Both water and chlorine penetration resistance tests showed a definite decrease in impermeability after exposure to high temperatures. The water penetration resistance tests further offered insight into the relationship between the exposure duration and degree of degradation.

These findings underscore the importance of developing methods to preserve PC's desirable properties when exposed to elevated temperatures. Thus, investigating methods for protecting PC from exposure to elevated temperatures and/or improving its inherent fire resistance is crucial.

8. PROPOSED IMPROVEMENT TO FIRE RESISTANCE OF PC OVERLAYS

As noted from the test results presented in Chapter 7 of this report, PC degrades rapidly on exposure to extreme temperatures from vehicle fire incidences. This necessitates the development of strategies/methods to improve the fire resistance of the material and/or to mitigate its exposure during vehicle fires. This section outlines the design and testing of a fire-resistant mix to mitigate the effect of vehicle fires on PC overlays.

8.1 Design of Mitigation Strategies

Several solutions have been proposed for the improvement of PC's fire resistance in past studies. These methods have generally centered around adding fire resistant materials to the PC mix prior to casting. While such methods have shown varying degrees of success, they do not address a critical issue. Some PC overlays are already cast in place and thus such solutions would not work for them. In addition, the change in the properties of the PC which make them viable for such applications could be such that the material would no longer be attractive for such applications.

To this end, another path was explored in this study. This aimed to limit the exposure of the existing PC overlay to the heat from the vehicle fire. To do this, an intumescent coating was designed to be applied over the existing overlay. This is the most viable solution to test as it can be used over already existing PC without requiring the replacement of the entire overlay. PC overlays are usually finished by the application of finishing sand over them, which is held in place by the excess resin from the PC mix. As such, this application of finishing sand could be preceded by the application of the intumescent blend of the resin primer and the fire-retardant materials. The fire-retardant materials used for this purpose are expandable graphite, calcium carbonate, and aluminum trihydrate in a mix ratio suggested in previous studies involving the use of this material for developing an intumescent fire-retardant polymer resin adhesive [53]. Table 8.1 shows the mix ratio for the materials to make up the intumescent layer.

Table 8.1 Design mix for intumescent coating

Material	Percentage by weight (%)
Resin + MEKP	70
Expandable graphite	10
Aluminum trihydrate (ATH)	15
Calcium carbonate ($CaCO_3$)	5

The resin used was the same polyester polymer resin (Kwik Bond PPC 1121) used in the overlay for the slab where the vehicle fire was carried out. The initiator/hardener used (MEKP-9) was also the same as used in the PC overlay for the vehicle fire test. The expandable graphite used was Grade 3772 expandable graphite obtained from Asbury Carbons. This material begins char formation at about 190^{o}C, a nominal size of 300 μm, a carbon percentage of 98%, and an expansion ratio of 300:1 cc/g. The aluminum trihydrate used was SB-36 obtained from Huber Engineered Materials, with a particle size of 25 μm. The calcium carbonate used was Now calcium carbonate. These materials were chosen to fulfill specific roles in the fire-resistant intumescent material. The expandable graphite expands on exposure to heat to produce a thermally insulating foam, which protects materials beneath it from the detrimental effects of the heat. The aluminum trihydrate, on the other hand, relies on endothermic decomposition when exposed to high temperatures, producing water, and removing heat from the system. Calcium carbonate, when exposed to heat, produces gases to displace oxygen and thus suffocate the fire. As such, the three

materials utilize different mechanisms to fight fires and elevate temperatures, and thus produce a synergistic effect in limiting the heat exposure of surfaces they are used to protect.

8.2 Testing Methodology

Twelve small slabs (each measuring 2 ft x 2 ft x 8 in) were cast and overlaid with PC in a manner similar to the large slab tested in the vehicle fire. In testing these slabs for improving the fire resistance, four were reserved to obtain cores without exposure to the fires for use in tests that require a process that does not involve heating the entire panels. Two of these four panels were overlaid with the intumescent layer and two were not and as such served as the control slabs. The remaining eight were earmarked for testing under elevated temperatures (four plain and four with the intumescent coating), with four tested using each of the exposure temperatures. Figure 8.1 shows the panels with and without the intumescent layers, respectively.

(a) (b)

Figure 8.1 Test slabs a) control slab without intumescent layer and b) slab with intumescent layer applied

Both the uncoated and coated specimens were exposed to two temperatures (300^{o}C and 500^{o}C) using heating rates similar to those from the vehicle fire test. A variety of performance tests (skid resistance, surface hardness, delamination, abrasion resistance, rapid chloride penetration, and water penetration) were carried out on the samples in a manner replicative of the test design for the larger slab. Table 8.2 below gives a breakdown of the tests.

Table 8.2 Test matrix for experiments

	Test	Specimen size	Ambient temp. samples		300°C exposure		500°C exposure	
			Plain	Intumescent layer	Plain	Intumescent layer	Plain	Intumescent layer
Non-destructive tests	Skid resistance	N/A	2	2	2	2	2	2
	Surface hardness	N/A	2	2	2	2	2	2
Tests on cores	Water penetration	4 in. dia x 4 in ht.	4	4	2	2	2	2
	Abrasion resistance	4 in. dia x 4 in ht.	4	4	4	4	4	4
Special samples	Rapid chloride penetration test	4 in. dia x 8 in ht.	6	6	3	3	3	3

The non-destructive tests (skid resistance, surface hardness, and delamination) were carried out on all 12 panels initially, and on eight panels after they were exposed to the elevated temperatures. The results obtained were analyzed by comparing the difference in how the surface behavior changed in response to exposure to high temperatures. The destructive tests, which involved collecting core specimens from the slabs, were carried out on separate slabs prior to and after the high temperature tests.

8.3 Results and Analysis

The results from the cores collected from the slabs that were not exposed to the heat were used in characterizing the initial properties of the overlay and compared with the results obtained from cores exposed to the different temperatures. This was done to characterize the change in properties due to exposure. A breakdown of the tests listed in Table 8.2 and their attendant results from the tests is given in the subsequent sections. Figure 8.2 shows the slabs after exposure to the heat. After subjecting the slabs to the listed temperatures, the slabs without the intumescent protective layer suffered visible extensive damage, as was notable by the charred marks on the slab.

(a) (b)

Figure 8.2 Control slabs after exposure to temperatures of a) 300°C and b) 500°C

At 300°C, represented in Figure 8.2a, the damage to the overlay is barely visible as a brown spot in the middle of the slab. On the other hand, after exposure to 500°C, as shown in Figure 8.2b, the damage is more extensive with a clearly visible charred area in the center of the slab.

For the slabs covered with the intumescent coating, a similar effect could be observed, albeit with the intumescent coating limiting the damage to the overlay. Figure 8.3 shows the slabs with the intumescent coating after heating.

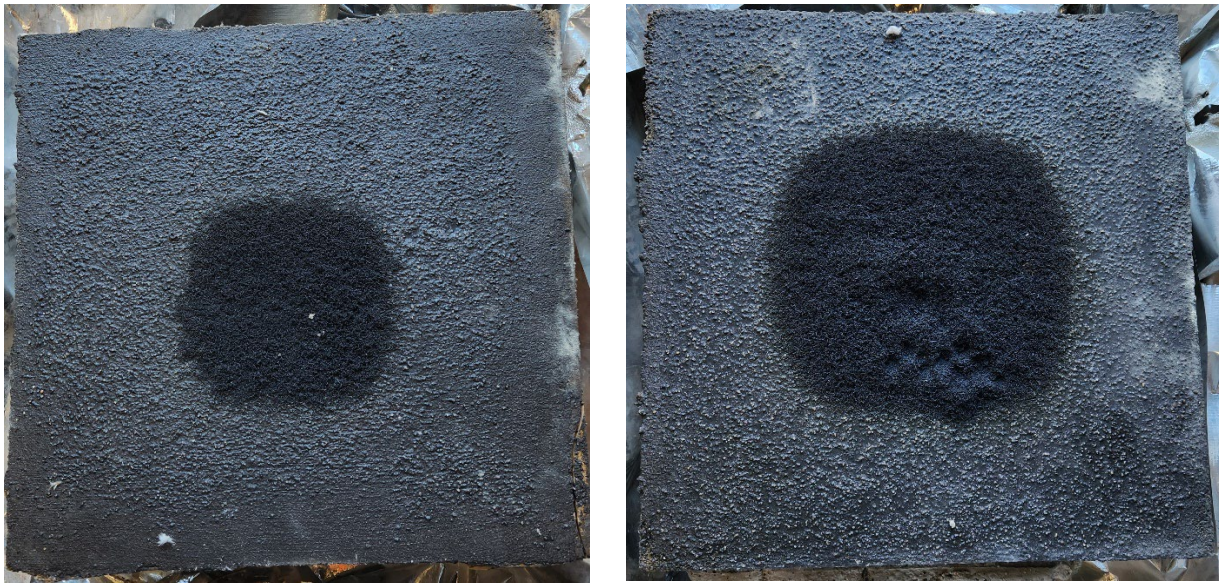

(a) (b)

Figure 8.3 Coated slabs after exposure to temperatures of a) 300°C and b) 500°C

Figure 8.3a shows the slab after exposure to the 300°C heat. The material in the center is the reaction of the intumescent layer. The expandable graphite had expanded and formed a protective layer over the overlay, preventing the heat from reaching it. This expanded layer is more extensive in Figure 8.3b, showing how the intumescent layer continues to protect the overlay as the temperature increases with more of the material expanding to prevent the heat from damaging the PC overlay. Figure 8.4 shows the slab after this expanded coating has been removed.

(a) (b)

Figure 8.4 Coated slabs without reacted coating after exposure to temperatures of a) 300ºC and b) 500ºC

Figures 8.4a and 8.4b reinforce the observations from Figure 8.3. It can be observed that the damage to the overlay from the heat is quite minimal, with some of the intumescent layer still present in slabs exposed to 300ºC. At the higher temperature (500ºC), the damage is greater, albeit mostly to the intumescent layer, with only limited exposure of the PC overlay visible. These initial observations lend credence to the idea that the intumescent layer could prevent damage to the overlay when the surface is exposed to elevated temperatures. To better characterize the effect of this overlaid layer, the tests described in Table 8.2 were carried out on core samples collected from the slabs or prepared independently to similar specifications. The results from these tests are described in the subsequent section.

8.3.1 Skid Resistance

Skid resistance tests were carried out on all the samples before and after exposure to the high temperatures. The results of the skid resistances of each slab before and after exposure are presented in Table 8.3.

Table 8.3 Skid resistance of exposed and insulated slabs

Test condition	Skid resistance (BPN)			Percent change (%)	
	Ambient temp.	300ºC	500ºC	300ºC	500ºC
Exposed	60.42	53.67	32.83	11.17	45.66
Insulated	55.92	47.67	52.75	14.75	5.66

The results in Table 8.3 show that the heat exposure resulted in a drop in skid resistance, which is similar to observations from the tests on the larger slab. However, this situation is mitigated with the inclusion of the insulated layer. On examination of the table, the skid resistance of the slabs tested at 300ºC seems to show a depreciation in performance with the application of the insulation layer. However, there is a caveat to this. The initial skid resistance used in making the comparison was the skid resistance obtained prior to the application of the insulation layer. On application of the layer, the skid resistance drop

significantly from an average value of 60.4 to 55.9. This value, while meeting the minimum acceptable threshold of BPN for road surfaces, indicates that the insulation layer may have some adverse effects on the overlay. This leads to a situation where after exposure to 300^{o}C, there is still some insulation over the surface, leading to a value of skid resistance that is much lower than the initial value prior to the application of the insulation. However, at 500^{o}C, all the insulation applied has reacted to the heat, exposing the overlay again. At this time, there is a small drop in the skid resistance of the surface (5.7%), which is quite minimal compared with the change in the skid resistance of the slab surface without the added insulation (45.7%). This gives an insight into the insulation's value in minimizing the effects of elevated temperatures on overlay surfaces.

8.3.2 Surface Hardness

Similar to the skid resistance, surface hardness tests were carried out on all the slabs prior to the placement of the insulation layer and prior to exposure of some of the slabs to heat. The results of the hardness tests before and after exposure are presented in Table 8.4.

Table 8.4 Surface hardness of exposed and insulated slabs

Test condition	Surface Hardness (RN)			Percentage change (%)	
	No heat	300	500	300	500
Exposed	51.79	50.83	37.87	1.85	26.89
Insulated	51.17	49.08	49.50	4.07	3.26

From the results shown in Table 8.4, the change in surface hardness of the overlay at 300^{o}C is quite negligible. This changes with the inclusion of the intumescent insulation layer with the surface hardness reducing. This scenario is similar to the observed results for skid resistance. This can be attributed to the expansion of materials in the intumescent coating on exposure to heat. The expansion creates a temporary barrier protecting the PC, which also has very limited surface hardness, from the heat. At 300^{o}C, this reaction is only partially complete, leading to the existence of a partially decomposed intumescent layer with minimum hardness. However, at 500^{o}C, the decomposition of the intumescent layer is more extensive, thus the surface hardness tested includes the now exposed overlay. At this higher temperature, it can be observed that there is very little change in the hardness (3.3%) compared with the sample without the protective layer, which recorded a 26.9% drop in hardness.

8.3.3 Water Penetration

With the water penetration tests requiring the testing of the same samples prior to and after exposure to elevated temperatures, eight cores were obtained for water penetration tests (four from the two panels without the intumescent layer and four from the panels with the intumescent layer). These samples were tested to obtain their individual coefficients of permeability. Afterwards, they were exposed to heating at the same rate as the slabs. To test them, each specimen was carefully wrapped in insulation with only the PC overlaid surface left bare to ensure that only this surface was exposed to the heat, in a manner comparable to exposing the overlay to a vehicle fire. After exposure, each sample was again tested to obtain its coefficient of permeability and the change in permeability. Figure 8.5 shows the cores after exposure to the elevated temperatures and Table 8.5 shows the results of the water penetration tests on cores collected from the slabs.

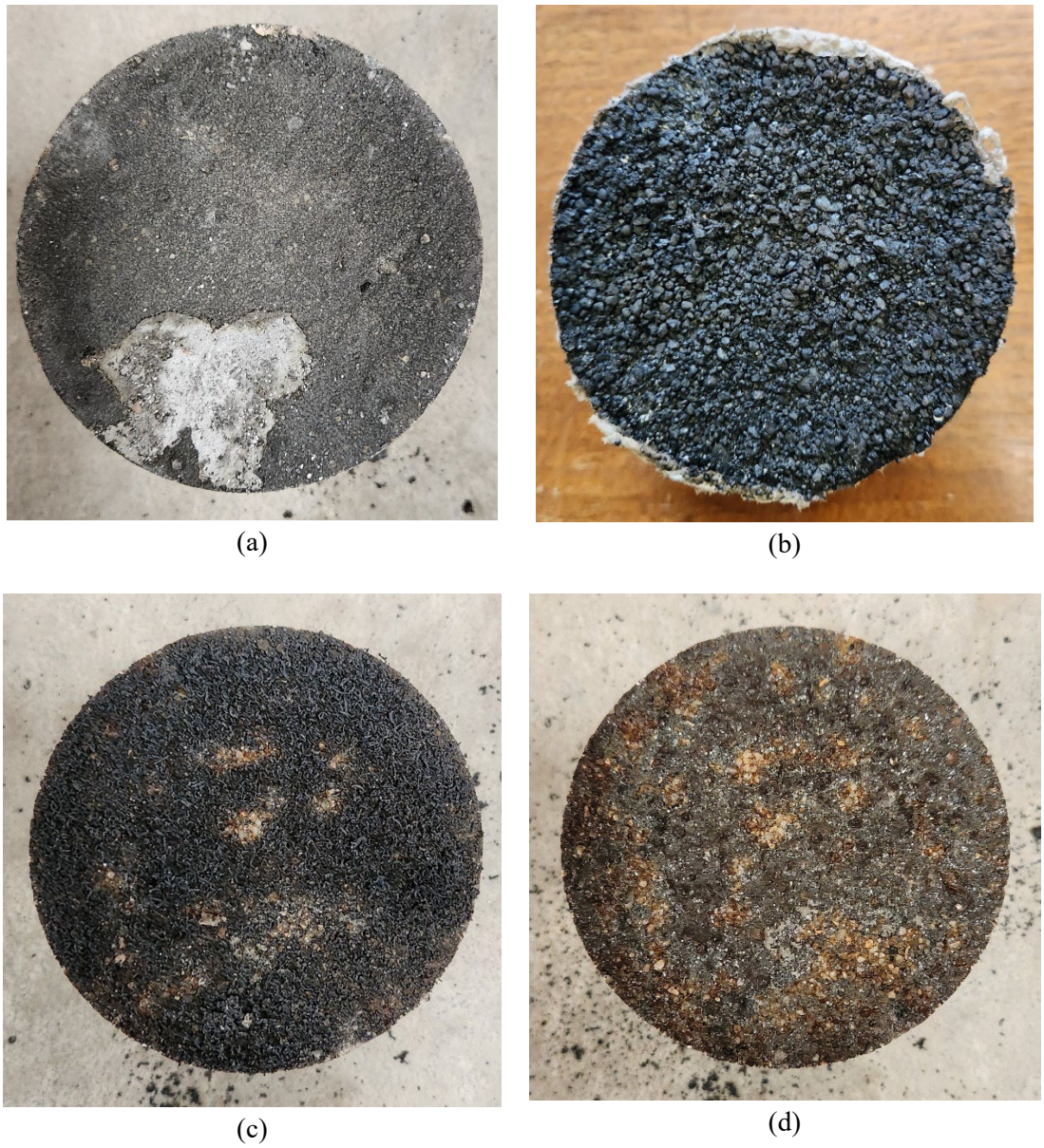

Figure 8.5 Core samples for water penetration a) control sample after exposure to 300°C, b) control sample after exposure to 500°C, c) coated sample after exposure to 300°C, and d) coated sample after exposure to 500°C.

Figure 8.5 shows that the core samples, which were not insulated (8.5a and 8.5b), sustained damage to the overlay as indicated by the extensive char over the surface. However, the core samples with the intumescent layer had the intumescent layer preventing extensive damage to the overlay. This is observed in Figures 8.5c and 8.5d where the intumescent layer withstood most of the heat, while remaining over the surface in Figure 8.5c and exposing the overlay in Figure 8.5d, albeit preventing damage to it.

Table 8.5 Coefficient of permeability of exposed and insulated slabs

Test Condition	Temperature (°C)	Sample	Coefficient of Permeability		
			Pre-fire (m/s)	Post-fire (m/s)	Percent change (%)
Exposed	300	1	6.12E-15	7.26E-15	18.57
		2	1.37E-14	1.55E-14	13.14
	500	1	1.47E-14	6.75E-14	357.89
		2	7.30E-15	3.24E-14	344.36
Insulated	300	1	6.37E-15	8.00E-15	25.60
		2	1.34E-14	1.47E-14	9.96
	500	1	1.30E-14	2.79E-14	115.28
		2	1.10E-14	2.50E-14	127.71

Table 8.5 indicates that across the different temperatures there is a very significant increase in the coefficient of permeability with the increase in exposure temperature. However, this increase, while similar for the specimens exposed to 300°C temperatures, dramatically diverges at 500°C. At this higher temperature, the core samples, which were not protected by the insulation layer, showed an average increase in permeability of 351%, almost 230% greater than the increase in samples protected with the intumescent coating.

8.3.4 Abrasion Resistance

The abrasion resistance tests were carried out on cores obtained from the slabs, which were not exposed to the elevated temperatures, as well as from those exposed to the high temperatures. Four cores were tested to obtain the pre-fire abrasion resistance of the overlay and four more were tested for the abrasion resistance of the overlay with intumescent coating. From the panels exposed to the elevated temperatures, 16 cores were obtained (four at each parameter as described in Table 8.2). Each of these were tested for abrasion resistance, and the results compared to determine the difference in the change in abrasion resistance between overlays with an intumescent layer and those without such a layer. Table 8.6 shows the results from the abrasion resistance tests.

Table 8.6 Abrasion resistance of exposed and insulated slabs

Test condition	Change in weight (g)			Percentage change (%)	
	Ambient temp.	300°C	500°C	300°C	500°C
Exposed	3.90	3.50	10.25	10.26	162.82
Insulated	3.90	3.75	3.00	3.85	23.08

From the table, note that the change in amount of material abraded from the surface of the specimens exposed to 300°C is lower than the material removed from the surface of the specimens not exposed to the elevated temperatures, albeit the difference is quite negligible. This difference can be attributed to differences in the surface finish for the different slabs, which resulted in small changes in the abraded materials that cannot be attributed to any intrinsic change in the properties of the overlay. However, on exposure to 500°C, the change in the amount of material removed from the samples not protected by the intumescent layer rose significantly by over 162%, while that for the samples protected by the intumescent layer rose by a much more modest 23%. These values again reinforce the value of the intumescent layer and its ability to limit the damage done to the overlay on exposure to elevated temperatures.

8.3.5 Rapid Chloride Penetration

The rapid chloride penetration tests require special cylindrical samples. As such, twelve 3 in. x 6 in. concrete specimens were obtained and covered with PC to make 4 in. x 8 in. samples. Six of these were covered in the intumescent layer similar to the covering of the slabs, and the remaining six were left plain. The results for RCPT tests on the samples without the intumescent layer are presented in section 7.7. Figure 8.6 shows the specimens before and after exposure to the elevated temperatures.

(a) (b) (c)

Figure 8.6 Control and coated cylindrical specimens for RCPT a) prior to testing, b) after exposure to 300^{o}C, and c) after exposure to 500^{o}C

Figure 8.6b and 8.6c show the contrast between the damage to exposed samples and those covered in a layer of the intumescent material. In Figure 8.6b, both specimens were exposed to temperatures of 300^{o}C, and extensive visible damage was not noticed in the material. However, on exposure to 500^{o}C, the control sample shows extensive fire damage with extensive charring visible on the surface. By contrast, the sample covered in the intumescent coating shows much lower levels of damage, buttressing the value of the intumescent layer in preventing damage to the overlay. To quantify the effect of the intumescent layer on the chloride penetration of resistance of the PC overlay, Table 8.7 shows the results of the RCPT tests for specimens of both types.

Table 8.7 Resistivity of exposed and insulated slabs

			Resistivity (kΩ-cm)		Percentage change
	Temperature (°C)	Sample	Pre-fire	Post-fire	
Exposed	300	1	671.25	490.38	26.95
		2	767.00	490.63	36.03
		3	719.13	501.33	30.29
	500	1	749.00	378.75	49.43
		2	745.13	355.75	52.26
		3	750.06	372.11	50.39
Insulated	300	1	770.81	593.63	22.99
		2	839.00	490.75	41.51
		3	804.91	542.19	32.64
	500	1	863.38	505.00	41.51
		2	908.88	491.25	45.95
		3	886.13	498.13	43.79

From Table 8.7, it can be noted that the percent change in resistivity of the specimens, both insulated and exposed, change relative to the exposure temperature. This change does not differ greatly between the exposed and coated specimens, with only an average reduction of about 7% in the resistivity of the bare samples compared with the coated samples after exposure to 500°C. This indicates that at temperatures up to 500°C, the addition of an intumescent coating will not significantly impact the resistivity of the overlay. However, the trend of divergence in the resistivity of coated and uncoated samples (with the difference in average resistivity increasing from under 1% to about 7%) is indicative of the value of the coating to help limit the damage to the overlay, albeit relatively small in the RCPT. With the RCPT continually staying above the limit of 254 kΩ-cm that would indicate a porous material, this small change seems insignificant but could subsequently be the difference between an overlay that could stay in service and one that would need replacing.

9. CONCLUSION

This study aimed to investigate the impact of vehicle fire exposure on civil infrastructure, particularly PC when used as overlay on concrete bridge decks. PC is desirable due to its excellent properties, such as its high bond strength with substrate concrete, short curing times, good water and chlorine resistance, and excellent skid and abrasion resistance. To understand how these properties change after exposure to fire, a vehicle fire test was carried out on a reinforced concrete slab overlaid with PC, replicating an accidental vehicle fire outbreak on a bridge deck with a PC surface. The exposure of the bridge deck to the vehicle fire was studied and the performance of the PC overlay before and after the fire was evaluated and compared.

A number of characteristics were noted from the vehicle fire, which only lasted for about 225 seconds. The temperatures collected from different locations in the vehicle and over the panel revealed that the temperatures from such scenarios could be quite extreme, with some of the thermocouples installed in the vehicle recording temperatures around 1,200^{o}C, while the maximum temperature recorded on the panel was 744^{o}C. In addition to the extreme temperatures, a recorded heat flux of up to 47.5 kW/m^2 at 12 ft from the vehicle center highlights the risk posed by vehicle fires. This elevated heat flux suggests that the damage by a vehicle fire could extend beyond the pavement, posing a threat to surrounding infrastructure such as suspension bridge cables. Moreover, in wildland areas, there is even a possibility of igniting wildfires if the bridge is located in close proximity to such regions. This risk is expected to rise in the future as the number of electric vehicles (EVs) on the road continues to increase. Handling EV fires pose unique challenges compared with fires involving traditional vehicles, as they tend to be more difficult to extinguish and often have a longer duration, potentially resulting in greater damage to civil infrastructure.

Prior to and after the vehicle fire, a series of experiments, including both non-destructive and destructive tests, were carried out on the panel to characterize the effects of the vehicle fire on the PC overlay. The results showed that even a short exposure to elevated temperatures from a fire could lead to marked degradation in the properties of PC overlays. Degradation was evident in areas exposed to high temperatures, affecting surface hardness, skid resistance, abrasion resistance, bond strength, water penetration resistance, and chlorine penetration resistance. Additionally, delamination between the overlay and the underlying substrate concrete was observed. These results indicate that PC overlays are susceptible to high temperatures and fire, leading to a loss of desirable properties.

After the vehicle fire tests, some methods of improving the fire resistance of the PC overlays were considered. These methods included adding fire retardant materials into the PC design mix, and/or applying a fire-resistant coating over the PC overlay when deployed. The first option of including fire retardant materials was jettisoned in this study as it could not be used for already existing PC. To this end, the method of the application of a fire-resistant coating to PC was investigated further. A fire-resistant mix, which is compatible with PC, was first identified. This mix included three materials, each of which resists fires via a different mechanism. These materials were blended into the PC binder resin and applied as a coating over small test slabs overlaid with PC to the same specifications as the slab used in the vehicle fire test. Controlled testing of these slabs for the same performance tests carried out on the larger slab indicated that the intumescent layer does help prevent damage to the PC overlays from fires by reacting at elevated temperatures to create an insulative layer, thus preventing the PC from significant exposure to the temperatures. The results from these tests indicate this to be a viable method for protecting PC from the effects of extreme temperatures. In addition, this material can be deployed either at construction or at any time in the life of the PC member, thus increasing its viability for use.

As the use of PC overlays becomes more prevalent, it is crucial to evaluate their performance in fire-related scenarios and establish strategies for mitigating their exposure to high temperatures or slowing down their degradation under these conditions. As an initial solution, an intumescent coating has been proposed and its efficacy in safeguarding the PC during a fire demonstrated. Nevertheless, it is important to recognize that implementing such a method could potentially raise the overall cost of the PC. Therefore, any deployment of this proposed solution should also encompass an assessment of its cost implications on an already expensive construction material.

10. REFERENCES

[1] U.S. Highway Vehicle Fires 1980-2020 | Statista n.d. https://www.statista.com/statistics/377006/nmber-of-us-highway-vehicle-fires/ (accessed September 20, 2022).

[2] United States Fire Administration (USFA). "Vehicle fires what you need to know." n.d.

[3] Allahvirdizadeh R., Rashetnia R., Dousti A., Shekarchi, M. "Application of polymer concrete in repair of concrete structures: A literature review." *Concrete Solutions* 2011:435–44.

[4] Phares B., Dulberg, J.M. "Polymer concrete overlay evaluation." Ames, IA: Iowa. Dept. of Transportation; 2016.

[5] Utah Department of Transportation. 2023 Standard Specifications for Roads and Bridges. Salt Lake City, Utah: Utah Department of Transportation; 2022.

[6] Gama, N. "Durability of epoxy polymer concrete overlays for bridge decks." Thesis. McGill University, 1999.

[7] Yeon, K.S., Kim, K.K., Kim, C.Y., Yeon, J.H. "Coefficient of thermal expansion of polymer concrete with different polymeric binders." *Adv Mat Res*, vol. 1129, Trans Tech Publ; 2015, p. 139–44.

[8] Utah Department of Transportation (UDOT). *Structures Design and Detailing Manual*. 2017.

[9] AASHTO Task Force 34. *Guide Specifications for Polymer Bridge Deck Overlays*. Washington, DC: American Association of State Highway and Transportation Officials (AASHTO); 1995.

[10] Dulberg, J.M., Phares, B. "Polymer Concrete Overlay Evaluation." Iowa. Dept. of Transportation; 2016.

[11] Fowler, D.W., Whitney, D.P. "Long-term performance of polymer concrete for bridge decks." vol. 423. *Transportation Research Board*; 2011.

[12] Ferdous, W., Manalo, A., Wong, H.S., Abousnina, R., AlAjarmeh, O.S., Zhuge, Y., et al. "Optimal design for epoxy polymer concrete based on mechanical properties and durability aspects." *Constr Build Mater* 2020;232:117229. https://doi.org/10.1016/j.conbuildmat.2019.117229.

[13] Jafari K., Tabatabaeian, M., Joshaghani, A., Ozbakkaloglu, T. "Optimizing the mixture design of polymer concrete: An experimental investigation." *Constr Build Mater* 2018; 167:185–96. https://doi.org/10.1016/j.conbuildmat.2018.01.191.

[14] ACI Committee 548. *Guide for the Use of Polymers in Concrete*. American Concrete Institute; 1997.

[15] Sprinkel, M.M. "Thermal compatibility of thin polymer-concrete overlays." *Transportation Research Record*, IV 1983; 76:64–73.

[16] Nizamoff, D., Hanson, M. "Rehabilitation of bridge I-585 on Augustine cutoff." TRB Annual Meeting, Transportation Research Board of the National Academies, Washington, DC, 2015.

[17] Fowler, D.W. “Polymers in concrete: A vision for the 21st century.” *Cem Concr Compos* 1999; 21:449–52. https://doi.org/10.1016/S0958-9465(99)00032-3.

[18] “Properties of Polyesters.” n.d. https://polymerdatabase.com/polymer%20classes/Polyester%20type.html (accessed September 20, 2022).

[19] Letsch, R. “Behaviour of polymers and polymer mortars at constant and changing temperatures.” Proceedings of the 10th International Congress on Polymers in Concrete, 2001.

[20] Vipulanandian, C., Paul, E. “Performance of epoxy and polyester polymer concrete.” *Materials Journal* 1990; 87:241–51.

[21] Pardo, A., Maribona, I.R.Z., Urreta, J., San Jose, J.T., Muguerza, A. “Influence of dosage and temperature on mechanical properties of polymer concrete.” Proceedings of the Eight International Congress on Polymers in Concrete, Oostende; 1995.

[22] Elalaoui, O., Ghorbel, E., Mignot, V., Ouezdou, M. B. “Mechanical and physical properties of epoxy polymer concrete after exposure to temperatures up to 250°C.” *Constr Build Mater* 2012; 27:415–24.

[23] Okamoto, K., Otake, T., Miyamoto, H., Honma, M., Watanabe, N. “Burning behavior of minivan passenger cars.” *Fire Saf J* 2013; 62:272–80. https://doi.org/10.1016/j.firesaf.2013.09.010.

[24] Taham, M.M.R., Genedym, M., Ohama, Y. “Polymer concrete.” *Developments in the Formulation and Reinforcement of Concrete*, Elsevier; 2019, p. 391–408.

[25] Niaki, M.H., Fereidoon, A., Ahangari, M.G. “Experimental study on the mechanical and thermal properties of basalt fiber and nanoclay reinforced polymer concrete.” *Compos Struct* 2018; 191:231–8.

[26] Haurie, L., Lacasta, A.M., Ciudad, A., Realinho, V., Velasco, J.I. “Addition of flame retardants in epoxy mortars: Thermal and mechanical characterization.” *Constr Build Mater* 2013; 42:266–70.

[27] Tonet, K.G., Gorninski, J.P. “Polymer concrete with recycled PET: The influence of the addition of industrial waste on flammability.” *Constr Build Mater* 2013; 40:378–89.

[28] Elalaoui, O., Ghorbel, E., Ouezdou, M. B. “Influence of flame retardant addition on the durability of epoxy based polymer concrete after exposition to elevated temperature.” *Constr Build Mater* 2018; 192:233–9.

[29] Mohammadyan-Yasouj, S.E., Ahangar, H.A., Oskoei, N.A., Shokravi, H., Koloor, S.S.R., Petrů M. “Experimental study on the effect of basalt fiber and sodium alginate in polymer concrete exposed to elevated temperature.” *Processes* 2021; 9:510.

[30] Golestaneh, M., Amini, G., Najafpour, G.D., Beygi, M.A. “Evaluation of mechanical strength of epoxy polymer concrete with silica powder as filler.” *World Appl Sci J* 2010; 9:216–20.

[31] Jafari, K., Tabatabaeian, M., Joshaghani, A., Ozbakkaloglu, T. “Optimizing the mixture design of polymer concrete: An experimental investigation.” *Constr Build Mater* 2018; 167:185–96.

[32] Muthukumar, M., Mohan, D. “Studies on polymer concretes based on optimized aggregate mix proportion.” *Eur Polym J* 2004; 40:2167–77.

[33] Ferdous, W., Manalo, A., Wong, H.S., Abousnina, R., AlAjarmeh, O.S., Zhuge, Y., et al. “Optimal design for epoxy polymer concrete based on mechanical properties and durability aspects.” *Constr Build Mater* 2020; 232:117229. https://doi.org/10.1016/j.conbuildmat.2019.117229.

[34] Seco, A., Echeverría, A.M., Marcelino, S., Garcia, B., Espuelas, S. “Characterization of fresh and cured properties of polymer concretes based on two metallurgical wastes.” *Applied Sciences* 2020; 10:825.

[35] Bulut, H.A., Şahin, R. “A study on mechanical properties of polymer concrete containing electronic plastic waste.” *Compos Struct* 2017; 178:50–62.

[36] Shokrieh, M.M., Heidari-Rarani, M., Shakouri, M., Kashizadeh, E. “Effects of thermal cycles on mechanical properties of an optimized polymer concrete.” *Constr Build Mater* 2011;25:3540–9.

[37] Vipulanandan, C., Paul, E. “Characterization of polyester polymer and polymer concrete.” *Journal of Materials in Civil Engineering* 1993; 5:62–82.

[38] Lokuge, W.P., Aravinthan, T. “Mechanical properties of polymer concrete with different types of resin.” Proceedings of the 22nd Australasian Conference on the Mechanics of Structures and Materials (ACMSM 22), University of Southern Queensland; 2013.

[39] Doody, M.E., Morgan, R. *Polymer-Concrete Bridge Deck Overlays*. Albany, NY: 1993.

[40] Maass, J. “How Polyester Polymer Concrete Highway and Bridge Deck Overlays Became ‘State of the Art.’” Special Publication 2003;214:39–50.

[41] Krauss, P. “Status of polyester-styrene resin concrete bridge deck and highway overlays in California.” Proc., 43rd Annual Conf, 1988, p. 1–7.

[42] Sprinkel, M.M. “Polymer concrete bridge overlays.” *Transp Res Rec* 1993;1392:107.

[43] Tabatabai, H., Sobolev, K., Ghorbanpoor, A. “Evaluation of Thin Polymer Overlays for Bridge Decks.” Milwaukee, WI: 2016.

[44] Sprinkel, M. “Nineteen Year Performance of Polymer Concrete Bridge.” Special Publication 1997; 169:42–74.

[45] Krauss, P., Klail, A., Maggenti, R. “Development history, specifications, and case studies of polyester polymer concrete for bridge deck protection.” 24th Annual International Bridge Conference, 2007.

[46] Smith, A. “Overlaying concrete bridge decks with polymer concrete.” *Concrete Construction* 1991; 13:325–32.

[47] Fowler, D.W. “Polymers in concrete: A vision for the 21st century.” *Cem Concr Compos* 1999; 21:449–52. https://doi.org/10.1016/S0958-9465(99)00032-3.

[48] ACI Committee 548. *Guide for Polymer Concrete Overlays*, American Concrete Institute Detroit; 1998.

[49] Marschall, J., Frederick, M. “Thermal degradation of polymer concrete.” *Constr Build Mater* 1987; 1:14–8.

[50] Reis, J.M.L. dos. “Effect of temperature on the mechanical properties of polymer mortars.” *Materials Research* 2012; 15:645–9.

[51] Ribeiro, M.C.S., Nóvoa, P.R., Ferreira, A.J.M., Marques, A.T. “Flexural performance of polyester and epoxy polymer mortars under severe thermal conditions.” *Cem Concr Compos* 2004; 26:803–9.

[52] Ribeiro, M.C.S., Pereira, C.M.C., Sousa, S.P.B, Nóvoa, P.R.O., Ferreira, A.J.M. “Fire reaction and mechanical performance analyses of polymer concrete materials modified with micro and nano alumina particles.” *Restoration of Buildings and Monuments* 2013; 19:195–202.

[53] Li, K., Li, Y., Zou, Y., Yuan, B., Walsh, A., Carradine, D. “Improving the fire performance of structural insulated panel core materials with intumescent flame-retardant epoxy resin adhesive.” *Fire Technol* 2022:1–23.

[54] Lomakin, S.M., Zaikov, G.E. “Ecological aspects of polymer flame retardancy.” vol. 10. Vsp; 1999.

[55] Administration USF. Highway Vehicle Fires (2008 – 2010) 2013; 13.

[56] Ahrens, M. “Highway vehicle fire data based on the experiences of US fire departments.” *Fire Mater* 2013; 37:401–12. https://doi.org/10.1002/fam.2146.

[57] Kildare., S., Digges, K., George, T., Kildare, S., Digges, K., George, T., et al. “Analysis of Fire Occurrence in Automotive Crashes Using NASS CDS Data (1995 – 2004),” “Analysis of Fire Occurrence in Automotive Crashes Using NASS CDS Data (1994 – 2004),” 2006.

[58] A., Tewarson, J.G. Quintiere, D.A. Purser. “Post Collision Motor Vehicle Fires.” vol. I. Charlottesville, VA: 2005.

[59] National Fire Protection Agency (NFPA). NFPA 1710, *Standard for the Organization and Deployment of Fire Suppression Operations*. 2009.

[60] Upson, R., Notarianni, K.A. *Quantitative Evaluation of Fire and EMS Mobilization Times*. 1st ed. Worchester, MA: Springer Science +Business Media; 2010.

[61] Okamoto, K., Watanabe, N., Hagimoto, Y., Chigira, T., Masano, R., Miura, H., et al. “Burning behavior of sedan passenger cars.” *Fire Saf J* 2009; 44:301–10. https://doi.org/10.1016/j.firesaf.2008.07.001.

[62] Sun Xuan, Wang Wandi, Li Yinqing, Zhao Kewei, Hu Yue. “Full-scale car fire experiment.” J Tsinghua University (Science & Technology) 2010; 50:10–3.

[63] Jiang, X.H., Zhu, G.Q., Zhu, H., Li, D.Y. “Full-scale experimental study of fire spread behavior of cars.” *Procedia Eng* 2018; 211:297–305. https://doi.org/10.1016/j.proeng.2017.12.016.

[64] Zhu, H., Gao, Y., Guo, H. “Experimental investigation of burning behavior of a running vehicle.” *Case Studies in Thermal Engineering* 2020; 22:100795. https://doi.org/10.1016/j.csite.2020.100795.

[65] Stevens, R.J. “Polyester polymer concrete for bridge deck overlays.” Dissertation. Brigham Young University, 2020.

[66] ASTM International. ASTM E303: “Standard Test Method for Measuring Surface Frictional Properties Using the British Pendulum Tester.” West Conshohocken, PA: ASTM International; 2022. https://doi.org/10.1520/E0303-22.

[67] ASTM International. ASTM C805: “Standard Test Method for Rebound Number of Hardened Concrete.” West Conshohocken, PA: ASTM International ; 2002.

[68] ASTM International. ASTM D4788: “Standard Test Method for Detecting Delaminations in Bridge Decks Using Infrared Thermography.” West Conshohocken, PA: ASTM International; 2007.

[69] ASTM International. ASTM C1583: “Tensile Strength of Concrete Surfaces and the Bond Strength or Tensile Strength of Concrete Repair and Overlay Materials by Direct Tension (Pull-off Method).” West Conshohocken, PA: ASTM International; 2013.

[70] ASTM International. ASTM D5084-16: “Standard Test Methods for Measurement of Hydraulic Conductivity of Saturated Porous Materials Using a Flexible Wall Permeameter.” West Conshohocken, PA: ASTM International; 2016.

[71] ASTM International. ASTM C944/C944M-19: “Standard Test Method for Abrasion Resistance of Concrete or Mortar Surfaces by the Rotating-Cutter Method.” West Conshohocken, PA: ASTM International; 2019.

[72] AASHTO. T-358: “Standard Method of Test for Surface Resistivity Indication of Concrete’s Ability to Resist Chloride Penetration.” Washington, DC: American Association of State Highway and Transportation Officials …; 2014.

[73] Jiang, X.H., Zhu, G.Q., Zhu, H., Li, D.Y. “Full-scale Experimental Study of Fire Spread Behavior of Cars.” *Procedia Eng* 2018; 211:297–305. https://doi.org/10.1016/j.proeng.2017.12.016.

[74] SBG01 heat flux meter | Hukseflux n.d. https://www.hukseflux.com/products/heat-flux-sensors/heat-flux-sensors/sbg01-heat-flux-meter (accessed December 19, 2022).

[75] ASTM International. ASTM C42/C42M: “Standard Test Method for Obtaining and Testing Drilled Cores and Sawed Beams of Concrete.” West Conshohocken, PA: ASTM International; 2020.

[76] ASTM International. ASTM 5048: “Standard Test Method for Permeability of Granular Soils (Constant Head).” West Conshohocken, PA: ASTM International; 2006.

[77] Weisenpacher, P., Glasa, J., Halada, L. “Automobile interior fire and its spread to an adjacent vehicle: parallel simulation.” *J Fire Sci* 2016;34:305–22.

[78] Shintani, Y., Kakae, N., Harada, K., Masuda, H., Takahashi, W. “Experimental investigation of burning behavior of automobiles.” 6th Asia-Oceania Symposium on Fire Science and Technology, Korean Institute of Fire Science & Engineering; 2004, p. 618–29.

[79] “Thermocouple Cold (Reference) Junction Compensation.” n.d. https://blog.beamex.com/thermocouple-cold-junction-compensation (accessed December 29, 2021).

[80] ASTM International. ASTM E563: “Standard Practice for Preparation and Use of an Ice-Point Bath as a Reference Temperature.” ASTM International West Conshohocken, PA, USA; 2022.

[81] “ITS-90 Table for Thermocouples Coefficients of Approximate Inverse Functions.” n.d. https://srdata.nist.gov/its90/type_k/kcoefficients_inverse.html (accessed December 29, 2021).

11. APPENDIX

A.1 Testing of Thermocouples in Concrete Cylinders

The constructed thermocouples were tested in concrete cylinders to determine their viability for use in concrete over time. To test them, three concrete cylinders (two 4-in. diameter and 8-in. height cylinders, and one 6-in. diameter and 12-in. height cylinder) were cast. The thermocouples were then inserted into each to about halfway down its height. The cylinders were then left to cure in plastic molds for 24 hours. After 24 hours, the cylinders were demolded and placed in a curing chamber to cure. Each day over the first seven days, the internal temperature was taken from both the thermocouple in the samples and the room to continually study the viability of temperature measurements from the thermocouple as the concrete cures.

Equipment used for the concrete cylinders

1. Ready mix concrete
2. Molds (two 4-in. and one 6-in. molds).
3. Four thermocouples.

After being cured for seven days, the samples were placed in an ice bath and allowed to sit. At daily intervals, the internal temperatures in the bath and from the thermocouples inserted into the samples were collected. Ideally, after some time, both these temperatures should be the same when the sample reaches equilibrium. Also, afterwards, water was added to the ice with the samples to see how the temperatures change as the temperature of the water increases as the ice melts. Table 11.1 shows the temperatures of the different samples. Sample 1 represents the sample of 6-in. diameter and samples 2 and 3 represent the two samples of 4-in. diameter.

Table 11.1 Readings from thermocouples in concrete cylinders

Temperatures in curing chamber				
Days	Sample 1	Sample 2	Sample 3	Outside
1	17.7	16.2	15.5	19
2	20.6	20.6	20.6	20.7
3	20.7	20.7	20.7	20.8
4	21.2	21	21	19.2
5	21.2	21	21	19
6	21.3	21	21	21.1
7	21.3	21	21	21.1
Temperatures in ice bath				
Measurement	Sample 1	Sample 2	Sample 3	Ice bath
1	6.2	2.2	1.9	0.9
2	2.2	0.9	0.8	0.8
3	4	1.5	1.2	0.9
4	6.3	3.5	3.2	1
Temperatures in water				
Measurement	Sample 1	Sample 2	Sample 3	Water
1	7.2	4.6	4.4	1.3
2	18.4	18.2	18.1	18.1
3	21.9	22	22	22

From the results, it can be observed that while the samples were in the curing chamber, the temperatures fluctuated around the temperatures of the chamber. This is to be expected as the rate of carbon hydration had slowed down and thus the samples could be nearly at equilibrium with the chamber. On placing the samples in an ice bath, the temperatures dropped quickly. The temperatures in samples 2 and 3 (4 in. x 8 in. cylinders) soon reached an equilibria temperature with the ice bath. Sample 1 (6 in. x 12 in.) was still a little higher as it was a much larger sample. Beyond the second measurement, the ice started melting and the temperatures can be seen to rise as the temperature of the ice bath increased. The temperatures of the samples rose faster than that in the ice bath because, although slowed, the hydration process was still ongoing in the concrete as it had not reached its full strength. Similarly, on placing the samples in water, the temperatures rose rapidly until equilibrating with the temperature of the water.

From the analysis of the concrete samples under different conditions, it can be concluded that the thermocouples continued to effectively read the internal temperatures of the concrete over time. This indicates that thermocouples can be used to collect internal temperatures in concrete to a reasonable degree of accuracy as the concrete cures after casting.

A.2 Testing the Efficacy of Thermal Imaging for Capturing Delamination

A.2.1 Sample Exposed to Sunlight

In order to test the ability of the thermal camera to detect delamination in the bond between the polymer overlay and the concrete, a small test was conducted. A sample of concrete was cast, and a Pro-Poxy™ Type III DOT LT polymer overlay was cast on it to replicate the concrete panel with polymer overlay. This sample was then wrapped in mineral wool insulation leaving half the top surface of the polymer exposed. The sample was insulated in this manner to ensure that heat applied only penetrated the sample in one location (through the top). Half the top was also insulated in order to create a temperature differential across the surface to induce some stresses due to differential thermal expansion, which could lead to a delamination between parts of the overlay and the underlying concrete. Figure 11.1 shows the insulated sample prior to heating.

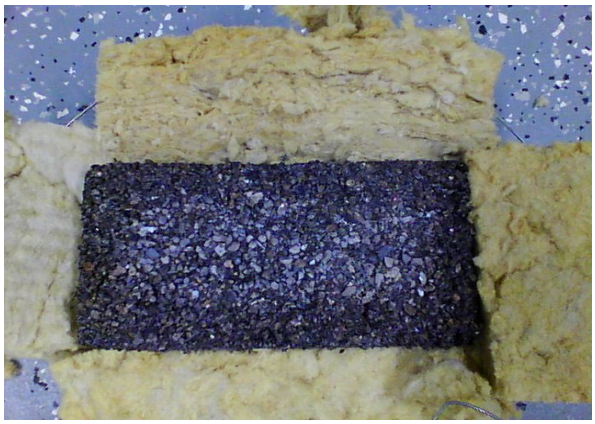

Figure 11.1 Sample with sides insulated to prevent heat input from sides

After insulation, the sample was placed in an oven and heated to about 140ºC for about four hours. The sample was then removed and the thermal insulation at the top surface taken off. The rest of the thermal insulation was left in place to ensure that the heat was only disseminated off the sample through the top surface. Figure 11.2 shows a thermal MSX image of the heated sample at the start of cooling. The thermal

MSX images are thermal images overlaid on regular images to allow for seeing some of the temperatures of a sample while also visually identifying the surface features at the locations.

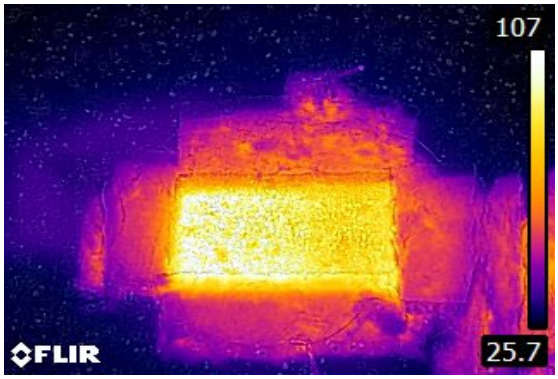

Figure 11.2 Thermal MSX image of sample after removing from oven

From Figure 11.2 it can be observed that the temperatures at the sample surface differ significantly. This can be attributed to the insulation placed on half the surface, leading to a limited amount of heat getting into half of the sample surface while the other half was exposed to elevated temperatures.

After cooling, the sample was again placed in the oven and heated to about 176^{o}F, this time without any insulation on the top surface. This was done in order to investigate if the thermal camera could capture differential thermal energy flow across the surface that would indicate the presence of subsurface defects. After heating, the sample was removed from the oven and several thermal images collected at intervals.

To enhance the contrast in the thermal images, a Gaussian smoothing process was applied to the thermal images collected as the sample cooled back to room temperature. This process involved using a Gaussian function in a convolution process to remove small details from an image and in this process eliminate noise. The process was applied to the thermal images in order to remove some detailed temperature differences caused by the uneven surface of the sample. After Gaussian smoothing, a k-means clustering process was used to group the surface temperature into three groups. These processes were carried out to determine if there was some delamination captured in the cooling phase by the thermal images, and if such delamination could be isolated using the image processing steps. Some of the collected images and the corresponding processed images are shown in Figure 11.3.

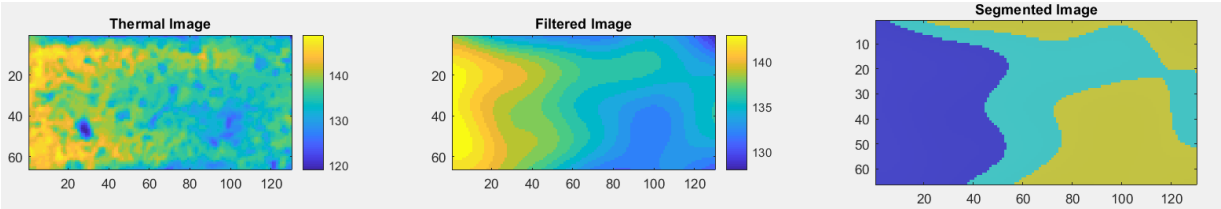

149°F

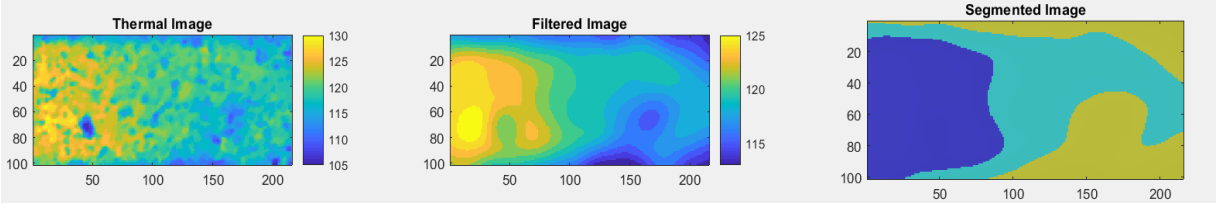

129.92°F

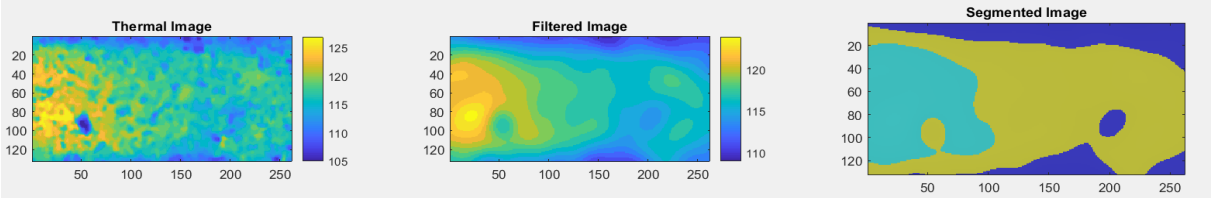

125.06°F

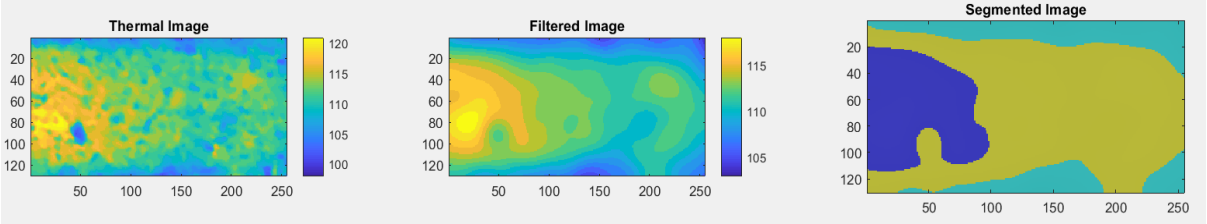

120.02°F

Figure 11.3 Thermal, filtered, and segmented images of sample surface at different temperatures

As seen in Figure 11.3 images, there is significant difference in the temperature between both parts of the surface. The part of the surface that did not initially have thermal energy applied on it to induce delamination seems to lose its heat faster than the region which had delamination induced. This is an indicator of a change in the underlying characteristics of part of the surface, which could possibly include delamination. In addition, as the sample cooled, a section of the sample was shown to be a consistent hot spot, indicating the presence of subsurface characteristics leading to the slowed down loss of thermal energy from this region. The images filtered using the Gaussian smoothing operator better delineate this region, and the clustered and segmented image shows the clear presence of three different clusters, indicating the difference in temperatures at both sides of the sample and an intermediate region in between.

To replicate the results in Figure 11.3, at temperatures closer to those we can expect in field conditions, a similar test was carried out. However, in the second test, the samples were only heated to about 122ºF, and for a short 15-minute period. Figure 11.4 shows the results from this test.

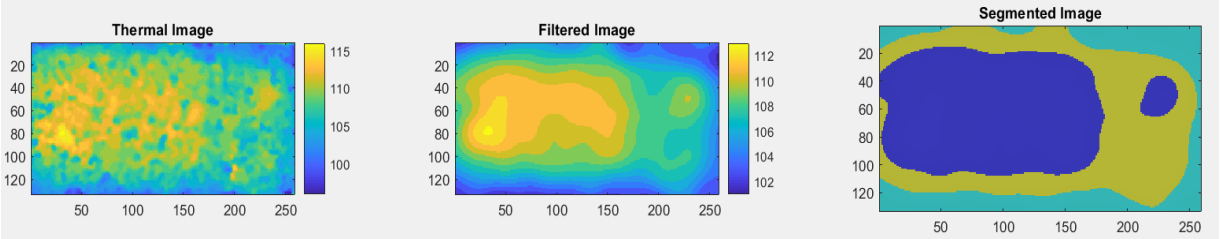

116.06ºF

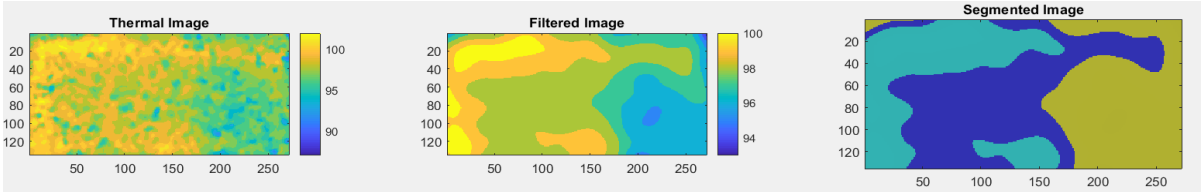

101.84ºF

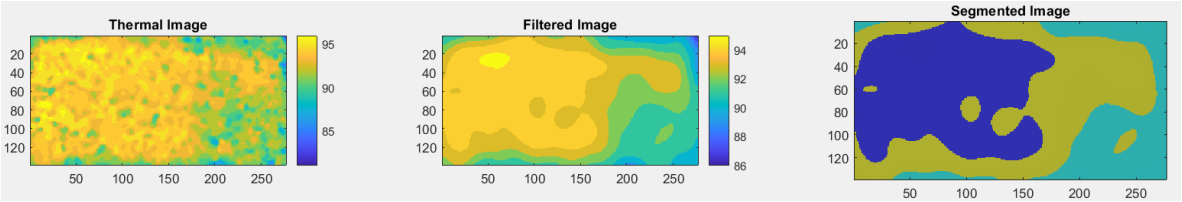

96.26ºF

Figure 11.4 Thermal, filtered, and segmented images of sample at lower heated temperatures

From the images in Figure 11.4, even at lower temperatures and shorter heating period, the differential cooling behavior between both halves of the sample is quite obvious. This again reinforces the idea that there has been some change in the structure of the overlay leading to a reduced rate of thermal change in the part of the sample that was initially exposed to elevated temperatures. From the images taken after removing the sample from the oven (temperature at 116ºF), the small region showing differential changes in thermal energy is quite obvious. However, as the sample cools down, this area becomes less visible and merges with the area around it, although the difference in thermal behavior of the two halves is still quite obvious.

These tests indicate that the thermal camera used (FLIR E8), even with its limitations (low thermal sensitivity of 0.06ºC and no video capabilities), can still capture differential thermal behavior in the concrete sample, which may be indicative of delamination between the overlay and the concrete substrate. However, this temperature differential does not show up at lower temperatures. As such, it may be necessary to have the sample remain heated at temperatures similar to field temperatures for an extended period (about three hours as specified in ASTM D4788). This may be necessary as the concrete has relatively low thermal conductivity and may not have absorbed the thermal energy adequately. As such,

the thermal energy may have been mostly concentrated in the overlay and quickly got expelled, thus not allowing the differential loss of thermal energy at different locations on the surface to be captured at the lower temperatures.

To better simulate expected field conditions, the sample was again heated in the oven to about 113ºF for an extended period of four hours. After heating, several images were collected as the sample cooled to room temperature. Figure 11.5 shows the resulting thermal images and the corresponding analyzed images. Temperatures listed for each set of images are the maximum temperatures of the sample at the time the thermal image was collected.

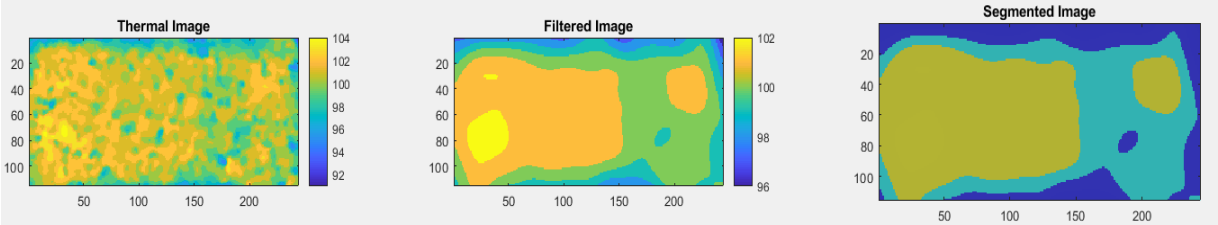

104ºF

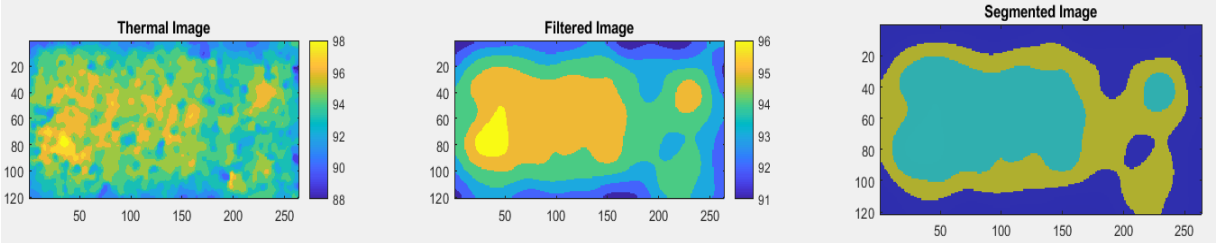

97.88ºF

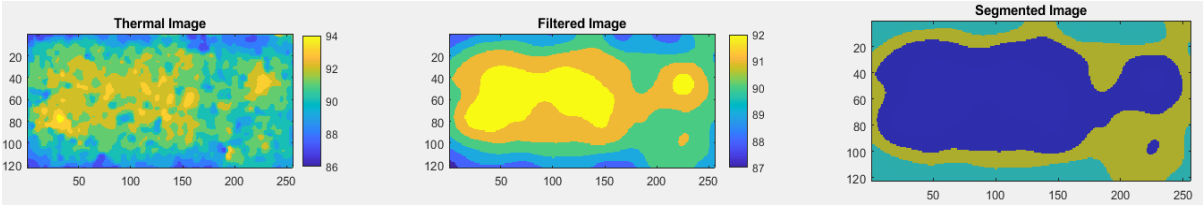

93.74ºF

Figure 11.5 Thermal, filtered, and segmented images of sample at heated temperatures similar to expected field conditions.

From the results in Figure 11.5, it can again be observed that even at these lower conditions, which are similar to what can be expected on the surface on the test panel after a hot summer day, the differential temperature patterns mirror those observed after heating the sample to elevated temperatures. The left side of the sample, which was initially heated to relatively high temperatures in order to induce delamination, continues to show a pattern of cooling at a slower rate than the right side, which can be assumed to still maintain its integrity. This may be indicative of subsurface delamination leading to a pocket of hot air between the overlay and the substrate concrete, which would help to maintain elevated temperatures.

A.2.2 Sample Exposed to Sunlight in Winter Condition

In attempting to replicate the conditions under which delamination will be studied in the concrete panel, the sample was exposed to direct sunlight from sunrise until the sun had passed the midday point. With the weather conditions at the time of the test (winter), the sample was placed in a display case and wrapped in insulation, leaving the top surface exposed. This was done to prevent the cold atmosphere from affecting the heating of the sample. The prepared sample was then placed in a foyer where it was expected to receive direct sunlight from sunrise until noon, when the sun would have passed beyond the area of the foyer exposed to the outside. Figure 11.6 shows the sample insulated and placed in the display case.

Figure 11.6 Insulated sample in display case

After heating, the sample was then allowed to cool and an image taken every hour as it cooled. Each of these thermal images was then processed in the same manner as was done with the images of the sample when heated in the oven. The thermal images and processed images are shown in Figure 11.7.

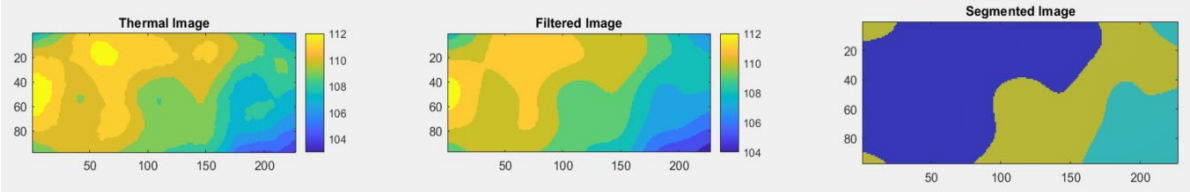

112.06ºF

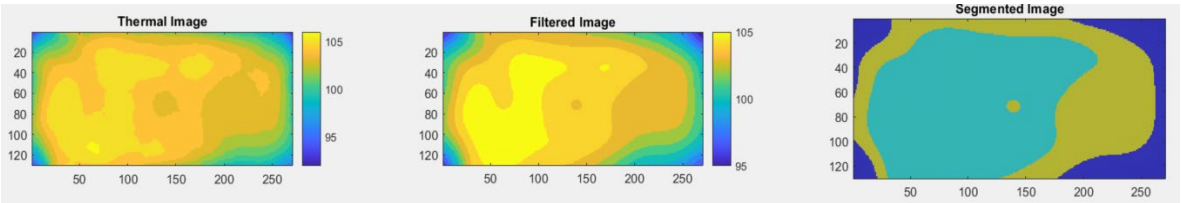

105.64ºF

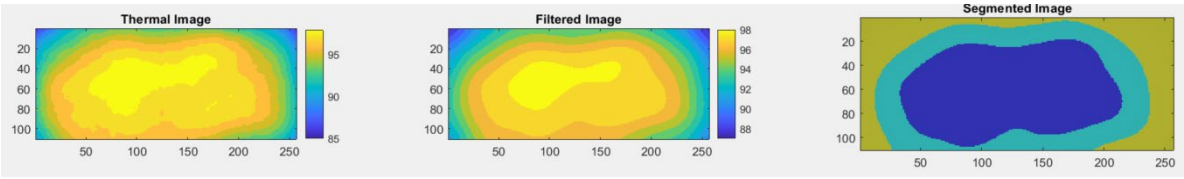

98.39ºF

Figure 11.7 Thermal, filtered, and segmented images of sample heated by exposure to sunlight

The results show there are some hot spots on the image similar to those from the previous tests. Ostensibly, these hot spots identify regions where delamination may have occurred between the overlay and substrate concrete leading to the creation of hot pockets when the sample was heated. This seemingly indicates that the thermal imaging process can capture subsurface delamination of a polymer concrete overlay and the concrete substrate even at relatively low temperatures.